



Regional modeling of the impacts of tidal flooding in the context of mean sea level rise on low-lying in the Global South

Thiago Cavalcante Lins Silva¹, Marco Túlio Mendonça Diniz^{1,3}, Paulo Victor do Nascimento Araújo², José Yure Gomes dos Santos³, Bruno Ferreira⁴, Jucielho Pedro da Silva^{3,5}

5 ¹Department of Geography, Federal University of Rio Grande do Norte, Natal, 59078-970, Brazil.

²Campus Macau, Federal Institute of Education, Science and Technology of Rio Grande do Norte, Macau, 59500-000, Brazil.

³Department of Geography, Federal University of Rio Grande do Norte, Caicó, 59300-000, Brazil.

⁴Institute of Geography, Development and Environment, Federal University of Alagoas, Maceió, 57072-900, Brazil.

⁵Department of Geosciences, Federal University of Paraíba, João Pessoa 58051-900, Brazil.

10 *Correspondence to:* Thiago Cavalcante Lins Silva (thiago.lins.115@ufrn.edu.br)

Abstract. This study assessed the risks and impacts of rising average sea levels on Brazil's semi-arid coastline in a low-lying coastal area with limited response potential, using freely available data and based on the central hypothesis that, even in conservative scenarios, there will be risks with significant impacts. The methodology integrated DEM calibration, geodetic validation of tide gauge data, flood modeling, and overlay with real estate grids to quantify damage. The results showed relative 15 stability of astronomical tides, with projected extremes of up to 2.975 m and 3.454 m, respectively, for a 20-year return period. Meteorological tides showed low values (\approx 0.11 m), although with episodic variability. The modeling indicated that up to 14% of the total area (about 730 km²) could be affected in extreme scenarios, with progressive flooding of solar salt pans and low-lying urban areas. Cities such as Areia Branca, Macau, and Porto do Mangue are at the highest risk, with a 60–80% probability 20 of flooded days in severe scenarios. Economic losses were estimated at approximately R\$ 36 million in residences (\approx US\$ 6.7 million) and R\$ 158 million in land (\approx US\$ 29 million), with Areia Branca being the most impacted municipality. Towns such as Barra, Cristóvão, and Baixa Grande also experienced significant risks and damage. The findings reinforce the usefulness of open data for regional risk analysis, even recognizing limitations in spatial resolution and vertical uncertainties. The methodology proved promising, replicable, and useful for supporting adaptive policies in regions with low institutional 25 technical capacity.

25 1 Introduction

Climate change is increasingly becoming a global emergency, with coastal areas serving as a confluence of highly energetic processes, making them focal areas for impact studies and adaptive planning (Rouse et al., 2016; Powell et al., 2018; Hinkel et al., 2018; Becker et al., 2023; Cabana et al., 2023). The consequences of climate change have several dimensions, such as 30 changes in terrestrial thermal patterns, changes and fluctuations in rainfall distribution, systematic imbalance in the trophic regime of coastal ecosystems, intensification of socio-spatial inequalities, recurrence and increased intensity of extreme events,



and rising average sea levels, which are the main global manifestations predicted by climate change (Arnell et al., 2019; González-Trujillo et al., 2023).

The mean sea level rise (MSLR), one of the most direct and significant consequences of the predicted changes, primarily threatens low-lying coastal environments through flooding and subsequent erosion (Le Cozannet et al., 2014; IPCC, 2022; 35 Scardino et al., 2022). Furthermore, recent projections indicate that even conservative scenarios could result in significant losses of territory in areas that are already vulnerable from both an environmental and social perspective (Almaliki et al. 2023; López-Dóriga and Jiménez, 2020). Such impacts compromise not only environmental integrity but also the socioeconomic security of coastal cities and populations (Araújo et al., 2021).

Developed coastal countries have increasingly implemented robust real-time monitoring and modeling systems, while many 40 naturally vulnerable regions, especially in the Global South, remain unengaged in risk assessments, mainly due to data scarcity and limited institutional and financial capacity (Nagy et al., 2019; Moser et al., 2019; Cabana et al., 2023).

Small and medium-sized coastal cities in semi-arid areas often lack the financial and technical resources to implement local 45 climate adaptation strategies (Boehnke et al., 2019; Fila et al., 2023; Olczak & Hanzl, 2025). In Brazil, the northern coast of the state of Rio Grande do Norte is an example of this vulnerability. The region is composed of economically fragile municipalities located in low-lying coastal areas (Aguiar et al., 2019), where tidal dynamics cause recurrent flooding (Araújo et al., 2021; Aguiar et al., 2019; Rabelo et al., 2023), a highly dangerous combination. The worsening of climate processes and the consequent rise in sea level may make the intrusion of marine processes a chronic problem, increasing socio-environmental stress and stress on poor urban infrastructure.

In this scenario, modeling for a regional context emerges as an interesting, viable, and low-cost approach to assess current and 50 future exposures, provided that the data used are properly validated, geodetically consistent, and considering vertical errors when associated with global Digital Elevation Models (DEMs) (Muench et al., 2022). without careful validation, there may be an overestimation of flood-prone areas (Vernimmen & Hooijer, 2023). Although these products have natural limitations in terms of spatial resolution, their wide availability and scalability make them useful tools in areas with technical and financial constraints (Ekeu-wei & Blackburn, 2018).

55 The central scientific question of this study is the construction of regional MSLR projection scenarios for the Brazilian Semi-Arid Coast (BSC), using open or low-cost aggregated data and mechanisms already implemented by the Brazilian Government to project scenarios from various sources, with the aim of identifying potentially impacted areas along the coastline. The starting point is the hypothesis that, even under the most conservative scenarios, there will be impacts on homes and land in various municipalities, creating endemic risk zones with high financial damage to major cities and other regions.

60 The study strategically sought to provide initial, yet applicable, input for regional and municipal flood management by fulfilling the following objectives: (I) mapping areas susceptible to tidal flooding under the current regime; (II) analyzing the frequency of flooding using historical data series; (III) analyzing multiple MSLR projections and their frequencies; (IV) assessing risk areas throughout the study area; (V) analyzing the impacts of risk areas, adopting as the study area the mouths of the Piranhas-Açu and Apodi-Mossoró rivers on the Brazilian Semi-Arid Coast.



65 Considering the high costs and low availability of detailed geospatial surveys, the proposed framework aimed to provide a holistic and integrated study with open data, designed using probabilistic logic based on abduction, which allowed for the preliminary identification of climate risks in the area, systematically updating previous projective studies (e.g.: Araújo et al., 2021; Aguiar et al., 2019; Santos et al., 2024). In addition, it established a general understanding and a starting point for the future development of high-resolution modeling for regional scenarios.

70 2 Study Area

The study area is located in the Costa Branca region, on the northern coast of the state of Rio Grande do Norte, a region characterized by a semi-arid hydrological framework, with salinized plains and low slopes (Diniz & Oliveira, 2016). Rainfall is concentrated in a few months of the year, mainly at the end of summer and beginning of autumn, alternating between years with rainfall above 800 mm and prolonged droughts (Medeiros et al., 2022; Kelly & Lucio, 2014).

75 The spatial area covers approximately 10,600 km², stretching along approximately 142 km of coastline, encompassing the estuaries of the Piranhas-Açu and Apodi-Mossoró rivers. The area partially includes the boundaries of the municipalities of Grossos, Tibau, Areia Branca, Porto do Mangue, and Macau (Figure 1), as well as villages near the coast. The municipalities in question have economic limitations and some are highly economically vulnerable, as verified by Macedo et al. (2025).

The area has a semi-diurnal mesotidal regime, with an average amplitude of around 2.66 m, reaching up to 2.85 m during 80 periods of more intense tides, such as in spring (Vital, 2009). The astronomical aspect is the controlling vector of the region's hydraulic dynamics, directly influencing coastal morphodynamics and depositing several sandbanks. In addition, the sector is influenced by waves from the northeast and east, with heights varying between 10 and 80 cm and average periods between 4 and 8 seconds (Vital et al., 2011; Barbosa et al., 2018).

The predominant land use is characterized by the production of sea salt in several evaporation ponds, which is the main 85 economic activity in the region (Diniz et al., 2015). The production process takes advantage of the flat environment of the hypersaline plains, high rates of potential evapotranspiration, and semi-arid hydroclimatic regime to produce sea salt (Diniz et al., 2017), making it the largest salt producer in Brazil.

The area is located in a low-lying coastal region (Eduardo et al., 2025), which is naturally vulnerable to flooding (Souza et al., 2021), a recurring phenomenon that has been documented in several publications (Aguiar et al., 2019; Araújo et al., 2021; 90 Rabelo et al., 2023; Silva et al., 2024). Low-lying coasts represent only about 2% of the world's coastlines (Nicholls et al., 2007), which makes the study area highly rare and exceptional. Due to their exceptional nature, these areas are frequently studied in international studies that seek to analyze the risks associated with this condition (Nicholls et al. 2007; Marfai & King, 2007; Dwarakish et al., 2009; Nicholls and Cazenave, 2010; Darsan et al., 2013; Boori et al., 2012; Busman et al., 2016; Stephens et al., 2021; Su et al., 2024), which makes the present study feasible and appropriate.

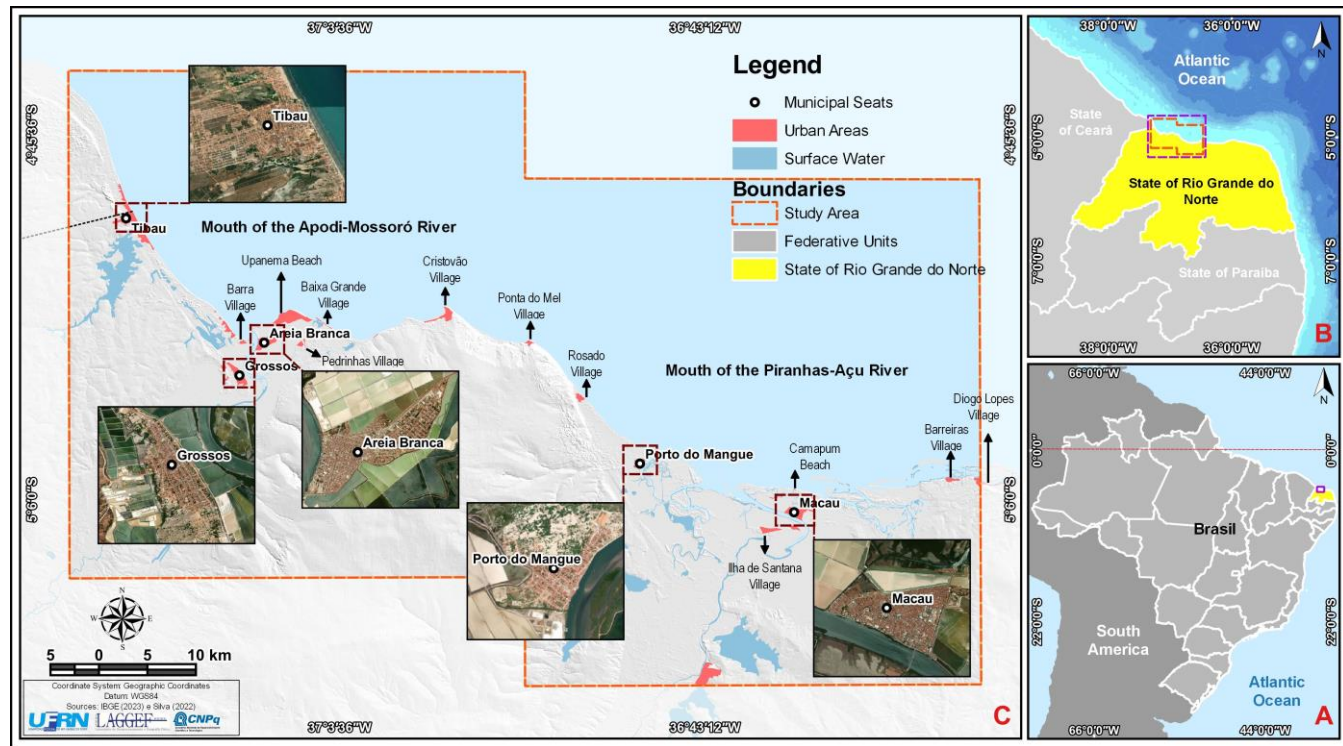


Figure 1: Study Area, with emphasis on the main urban centres in the area under analysis, the proximity to waterways is notable. Map prepared by the authors using data from IBGE (2023) and basemap data from Bing Maps (© Microsoft).

3 Material and methods

100 This study used the concept of risk as its central matrix, understood as the function between hazard and vulnerability (Kron, 2005; Wisner et al., 2012) (Eq.1), articulating physical, environmental, and social dimensions of the analyzed territory. Risk in this perspective is understood as a socio-environmental construct, influenced by both natural factors and social and territorial inequalities (Blaikie et al., 1994; Smith, 2001; Turner et al., 2003). The study area in this condition is understood as a region exposed to climate hazards due to its condition of human occupation (McGranahan et al., 2007; Vousdoukas et al., 2018). The 105 operationalization of the concepts guided the methodological discussions.

$$\text{Risk} = \text{Hazard} \times \text{Vulnerability}, \quad (1)$$

The methodology employed was designed in four main stages: (I) data collection; (II) data processing and validation; (III) processing and modeling; (IV) data analysis; (V) MSLR modeling; (VI) construction of the tidal flood risk map and identification of impacts. The stages and their sequence were designed with a view to achieving the objectives and resolving 110 scientific issues.



3.1 Data collection (I)

Data collection began with a systematic literature review on climate change, MSLR, and coastal risk modeling. The purpose of this review was to provide a theoretical basis for the research, identifying the main concepts, methodologies, and gaps in the literature. Next, the data necessary for the construction of the model were collected: (a) acquisition of altimetric data derived from freely accessible global DEMs; (b) survey of geodetic control points for DEM calibration; (c) obtaining historical tide gauge records; (d) compilation of MSLR scenarios and future projections, as established by leading scientific reports, such as IPCC projections; (e) land use data; and (f) urban data.

The spatialization of the main data is presented in Figure 2.

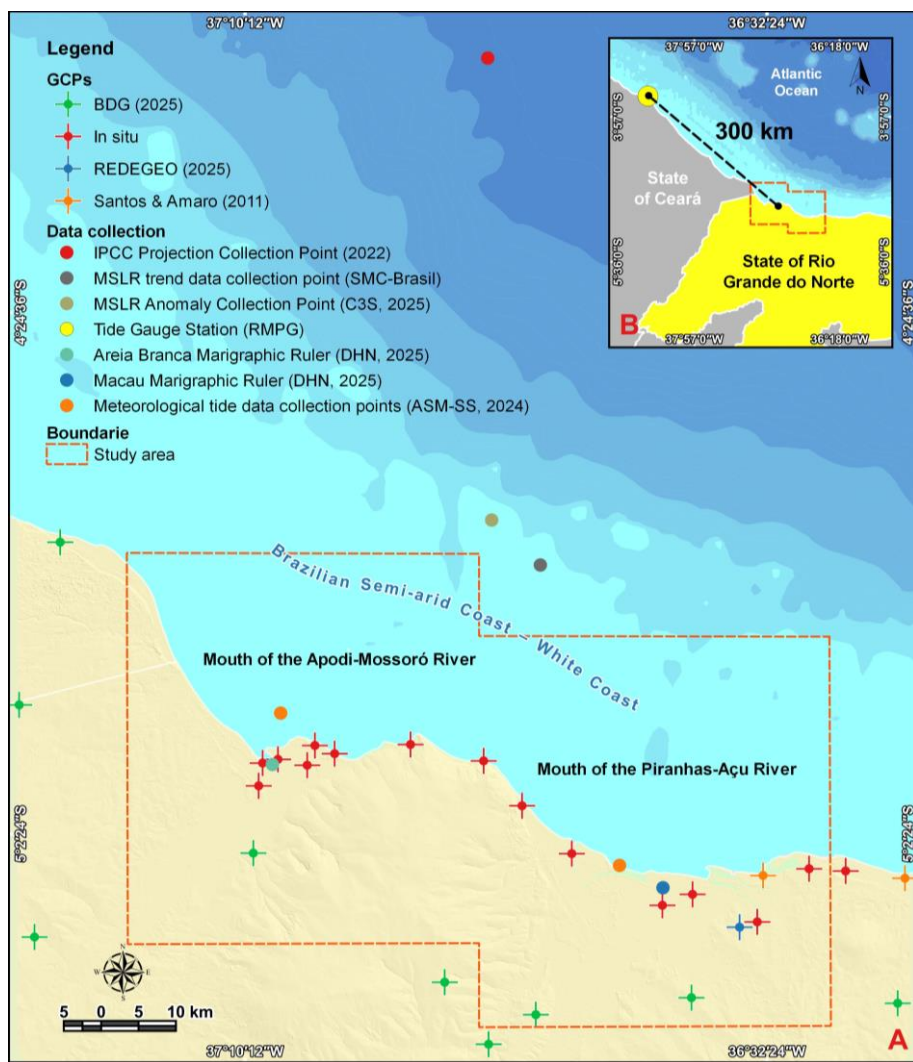


Figure 2: Spatialization of data collected and used in the study. A - context of the study area with the nearest data collection points; B - map showing the location of the RMPG tide gauge station. Map prepared by the authors (2025).



3.1.1 Elevation data

125 The DEM used in this study was the Copernicus DEM (COPDEM), a free global model derived from the TanDEM-X mission, launched in 2010. COPDEM was developed under the coordination of the European Space Agency (ESA) as part of the European Union's Copernicus Program (ESA, 2021) and has a spatial resolution of 30 meters.

For this study, the data were obtained via ESA's open access platform, with a specific cutout for the area of interest. COPDEM was chosen due to its proven ability to accurately represent land surfaces, especially in flat environments. In preliminary tests 130 with geodetic control points, the product presented, for the analytical cutout, a native Root Mean Square Error (RMSE) of 0.643 m, a value much lower than the nominal vertical error indicated by the manufacturer (≈ 4 m), confirming its suitability as an altimetric base in areas with low data availability.

3.1.2 Geodetic control points (GCPs)

In the survey of GCPs, valid geodetic references were selected, forming a structured network with representative coverage of 135 the main sectors of the study area. In total, 28 level references were used: 10 points from the Geodetic Database (BDG, 2025) of the Brazilian Institute of Geography and Statistics (IBGE); 15 points surveyed in the field with a Real-Time Kinematic GNSS receiver (CHCNAV I90), in static 2-hour sessions; 2 points from Soares & Amaro (2011); and 1 point from REDEGEO (2025). The latter three were strategically inserted to fill geodetic gaps and increase altimetric reliability in the most sensitive coastal areas. These points were essential for the altimetric calibration of the DEM and for the geodetic adjustment of the tide 140 gauges used in the validation of astronomical data.

In this sense, for the present study, it was agreed to adopt normal altitude as the altimetric reference, ensuring geodetic consistency between the different data sets used.

3.1.3 Astronomical Tides (AT)

The astronomical tide base was obtained from deterministic forecasts by the Hydrography and Navigation Directorate (DHN), 145 derived from harmonic analysis of historical series from 1940 to 2025, with hourly intervals. Data were also collected from the tide gauges in Macau and Areia Branca, with a view to linking the data and validating them geodetically. In addition, technical visits were made to verify the integrity of the gauges and their link to local level references.

3.1.4 Meteorological Tides (MT)

The tide gauge data associated with storm events were obtained from the Yang et al (2025) database, derived from Global 150 Extreme Sea Level Analysis version 3 (GESLA-3) reanalysis data, with cross-validated meteorological data extraction, covering the period from 1940 to 2020. Two data points were extracted, one in Macau and the other in Areia Branca, in the middle portions of the estuaries.



The data were calibrated using meteorological tide data from SMC-Brazil (2025), called Global Ocean Surge (GOS), ensuring greater regional representativeness due to its adjustment based on several local tide gauges. The calibration consisted of a 155 statistical comparison between observed data and GOS, with correction by linear regression and bias calibration using the base data. The process resulted in a reduction in the under/overestimation of the data, promoting an adjustment of around 0.02 to 0.03 m, applied to the two series analyzed.

3.1.5 Projections for MSLR

The study systematized the main MSLR projections applicable to the study area, on global, intermediate, and regional scales, 160 with a time horizon to 2100.

On a global scale, climate projections from the Sixth Assessment Report (AR6) of the Intergovernmental Panel on Climate Change (IPCC, 2022) were used, adjusted and spatialized by the National Aeronautics and Space Administration (NASA, 2021), considering a 50% probability of occurrence in scenarios SSP1-1.9, SSP1-2.6, SSP2-4.5, SSP3-7.0, and SSP5-8.5. In addition, sea level anomaly (SLA) data from the Copernicus Climate Change Service (C3S, 2025) were incorporated, derived 165 from satellite altimetry from multiple missions (TOPEX-Poseidon, Jason-1/2/3, Sentinel-3, Sentinel-6, among others) for the period 1992 to 2024. From the western tropical Atlantic data grid, an average elevation rate of 4.06 mm/y was obtained, calculated via linear regression.

At the intermediate scale, the long-term trends of the SMC-Brazil obtained by Silva et al (2025) for the region were considered, calculated from astronomical (AT) and meteorological (MT) tides in the period from 1948 to 2008, with an average elevation 170 rate of 2.10 mm/y, resulting from linear regression adjustment.

At the regional level, data from the Permanent Tide Gauge Network for Geodesy (RMPG/IBGE) station in the city of Fortaleza, State of Ceará, about 300 km west of the study area, were used, whose consolidated averages (2008 to 2020) indicate a rate of 1.30 mm/y, representing the closest and most continuous instrumental record available.

3.1.6 Land use data

175 The land use and land cover data for this study were obtained from the MapBiomas project (2025), which annually maps land use dynamics in Brazil and other Latin American countries. The project uses Landsat images (30 m spatial resolution), processed with automated algorithms and validated by a broad collaborative network of experts to detect and correct inconsistencies. The methodological robustness and scientific credibility of the products ensure high reliability, making them widely applicable in environmental and territorial planning studies (Souza et al., 2020).

180 3.1.7. Urban data

Urban data on residential areas and land plots were collected for the study area on a scale of 1:500. The data were derived from a systematic survey using Unmanned Aerial Vehicles (UAVs) in the municipalities of the region under study.



3.2 Data processing and validation (II)

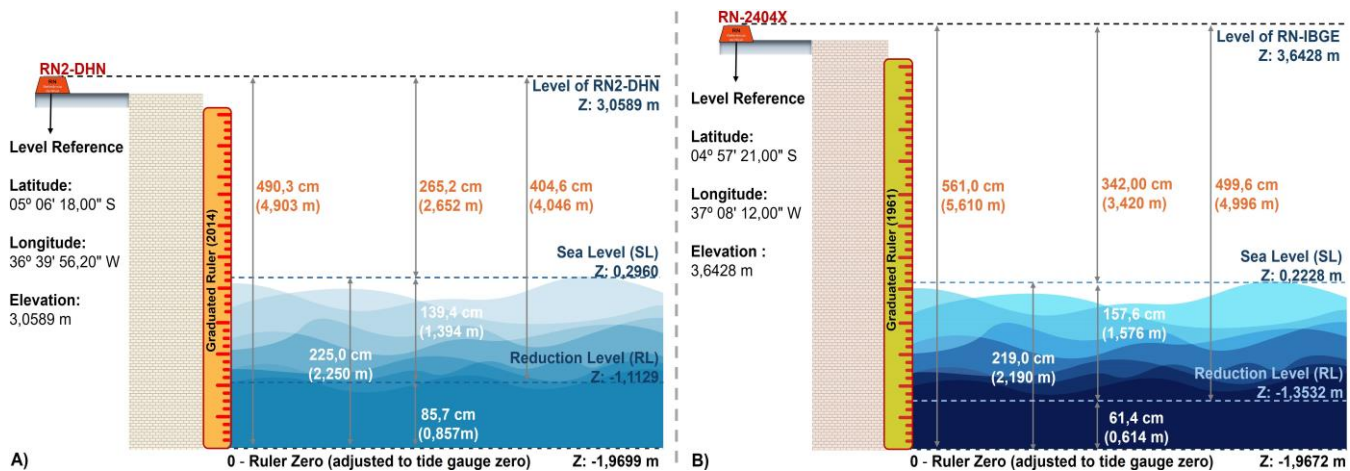
In data processing, COPDEM calibration was performed by comparing the model's altimetric quotas and GCPs, obtaining 185 metrics such as mean error, RMSE, and simple linear regression to derive a specific adjustment equation, following the approach recommended by Araújo et al. (2018). The application of the calibration equation (Eq.02) resulted in a significant gain in accuracy, with a 4% reduction in mean error and an overall RMSE of 0.612 m, a satisfactory value for global products. The distribution of errors by altimetric classes showed consistent behavior, with a standard deviation of 0.363 m and better performance at altitudes below 20 m, where the maximum RMSE was 0.30 m.

190 $Calibration\ Equation = 0.2041 + (DEM * 0.9939)$, (2)

Subsequently, the reduction level (RL) was adjusted to the Brazilian Geodetic System (SGB), a fundamental step in reconciling the astronomical data with the altimetric plane adopted in the study. This adjustment is necessary because tide gauge measurements originally follow the DHN's own reference system, which is geared toward measuring bathymetric depths for navigation and is incompatible with the geodetic system used in the study.

195 To equalize the vertical planes, two valid quoted points were used, adjusted to the SGB and referenced in SIRGAS2000, inserted near the tide gauge rules. In Macau, the point obtained by Araújo et al. (2021) was used, derived from the GNSS survey of the RN-2 (DHN) reference, in the vicinity of the Port of Macau. In Areia Branca, the official IBGE Level Reference (LR) (code 2404X) was used, geodetically linked to RN-3 (DHN), located next to the Port of Areia Branca, also used by Aguiar et al. (2019).

200 Based on the references surveyed, it was possible to calculate the RL elevations in relation to the geodetic plane, as illustrated in Figure 3, to Macau (Eq. 3) and Areia Branca (Eq. 4).



205 **Figure 3: Schematic representation of the tide gauge stations with the validated elevations and reference coordinates. A - Ruler associated with the Port of Macau; B - Ruler for the Port of Areia Branca. It can be seen that despite the unevenness, the reduction levels are close. Prepared by the authors using data from DHN (2025).**



The two reduction levels were essential for projecting the correction factor for the maximum astronomical values obtained, in order to weight the tide levels to the actual values in the preferred plane chosen.

$$Hm(RL) = H(LRm) - 4,046 \text{ m} = 3,0589 \text{ m} - 4,046 \text{ m} = -1,1129 \text{ m}, \quad (3)$$

$$210 \quad Hab(RL) = H(LRab) - 4,996 \text{ m} = 3,6428 \text{ m} - 4,996 \text{ m} = -1,3532 \text{ m}, \quad (4)$$

Where $Hm(RL)$ and $Hab(RL)$ are the Reduction Level (RL) quotas adjusted for Macau and Areia Branca; $H(LRm)$ and $H(LRab)$ represent the geodetic altitudes obtained by the level references near the tide gauges; and 4.046 m and 4.996 m are the official distances to the reduction level disclosed by the DHN for Macau and Areia Branca. The subtraction adjusts the tide plane to the geodetic system of the study.

215 The land use and land cover data obtained by MapBiomas underwent cross-validation, which was necessary to correct inconsistencies in the study area. Confusions between urban areas and water bodies were identified and adjusted, in addition to the resizing of salt ponds often misclassified as water. The procedure used a 1 km \times 1 km cell grid for detailed inspection, resulting in the correction of more than 80,000 pixels of incorrect classes.

Urban data were processed to estimate the value per square meter of the region through the systematic collection of real estate 220 advertisements using web scraping techniques, collecting more than 1,000 advertisements in the period 2023-2025, in a process similar to Jach, (2021), Bricongne et al. (2022), and Harten et al. (2020). In remote settlements, as there are no concrete market thresholds, interpolation with nearby areas was required for estimation. This estimate allowed us to construct real estate benchmarks used in the study.

3.4 Data analysis (III)

225 The tide analysis was conducted using statistical approaches applied to time series, aiming to understand the astronomical and meteorological influence and characterize extreme patterns for defining flood levels. The modeling considered the notion of total tide (FT), composed of astronomical (AT) and meteorological (MT) components, requiring independent analysis of both for more realistic projections.

The hourly AT and MT series were processed to extract daily and annual maximums. Descriptive statistics, the Mann-Kendall 230 trend test (Mann, 1945; Kendall, 1975), and the Morlet et al. (1982) wavelet transform were then applied, methods that allowed the identification of monotonic trends and cyclical patterns.

In the probabilistic stage, the Generalized Extreme Value (GEV) distribution was used to estimate non-exceedance 235 probabilities, and the Gumbel distribution was used to obtain the quotas associated with different return periods. The 20-year return period (RP20) was adopted as a reference for sea level rise scenarios, aiming at greater analytical consistency. This approach integrated natural variability into future projections, resulting in consistent and technically sound analyses.



3.5 Modeling of sea level rise (IV)

The MSLR modeling in this study was conducted based on two principles: event frequency, based on the recurrence of average annual floods; and total flooding, based on the maximum potential event. Both approaches allow for dealing with uncertainties associated with the occurrence of floods.

240 The study area was divided into two domains for modeling: Macau and Areia Branca, defined based on the availability of tide gauge data and the interpretation of marine process dominance proposed by Silva et al. (2025). The sectorization considered the change in the dynamic factors of hydraulic transport identified west of the village of Ponta do Mel, in Areia Branca, as a process divider, adopting it as the boundary between the two domains, but the interpretation will be integrated considering the study area as a whole.

245 The modeling was processed using the bathtub technique (passive model), which simulates, in a GIS environment, the expansion of the water surface over the DEM. This is a widely discussed method (Feenstra, 1998; Cartwright et al., 2008; Schmid, 2013; Yunus et al., 2016; Anderson et al., 2018; Gesch, 2018; Williams & Lück-Vogel, 2020; Terres de Lima et al., 2021; Shen et al., 2022; Juhász et al., 2023; Croteau et al., 2023; Sanders et al., 2024), with recent variations that include filtering by hydraulic connectivity and consideration of DEM uncertainties and MSLR projections. Despite limitations, such 250 as the absence of hydraulic flow simulation and hydrogeological constraints, it is a fast, low-cost technique suitable for screening vulnerable areas, especially in scenarios with technical and financial constraints. In addition, it is highly applicable in contexts of tide-dominated beaches.

Frequency modeling was implemented using a technique similar to Kaden's (2022) flood sector schematization, which compartmentalizes the DEM into altimetric levels and calculates the flood frequency based on daily time series of water levels.

255 The processing inputs include the series of daily total tide maximums (daily AT + daily MT), MSLR projections, calibrated DEM, and its RMSE, generating scenarios for each projection.

The total flooding followed the proposal by Araújo et al. (2021) and Aguiar et al. (2019), applying multivariate weighting based on the sum of hydrodynamic processes: DEM RMSE, MSLR projection, maximum meteorological tide (RP20), and maximum astronomical tide (RP20). The procedure was replicated for all scenarios, allowing for integrated analysis of coastal 260 dynamics and preliminary identification of associated problems.

3.6 Tidal flood risk mapping (V)

The risk map was constructed based on a probabilistic quantitative risk approach, defined by the relationship between hazard (destructive potential) and physical vulnerability (degree of environmental loss).

The hazard was classified based on total flood modeling in the different projected scenarios, segmented into five classes (0 to 265 5), from extremely low to extremely high (Table 1). Physical vulnerability was defined based on land use, grouped into five vulnerability units (0 to 5), ranging from “no vulnerability” to “extremely high”.



The weighted combination of these variables resulted in a tidal flood risk map, organized into five classes (0 to 25). Based on this, the practical implications associated with the defined risk limits were discussed. Finally, the map was overlaid with the region's real estate grid, quantifying the possible financial impacts and adjusting the losses per square meter by region.

270

Vulnerability Map			Hazard Map		
Categories of Use	Value	Class Name	Projected Scenarios	Value	Class Name
Urban Area	5	Extremely High	Present	5	Extremely High
Aquaculture	4	High	SMC-Brasil Trend	4	High
Pasture	3	Moderate	RMPG IBGE	3	Moderate
Mosaic of Uses	3	Moderate	SLA	3	Moderate
Other Temporary Crops	3	Moderate	IPCC SSP1-1.9	3	Moderate
Other Perennial Crops	3	Moderate	IPCC SSP1-2.6	3	Moderate
Forest Formation	2	Low	IPCC SSP2-4.5	2	Low
Savanna Formation	2	Low	IPCC SSP3-7.0	2	Low
Mangrove	2	Low	IPCC SSP5-8.5.	1	Extremely Low
Grassland	2	Low	Risk Map		
Hypersaline Tidal Flat	2	Low	Risk		Range
Beach, Dune and Sand Spot	1	Extremely Low	Extremely high		20 to 25
Other Non Vegetated Areas	1	Extremely Low	High		15 to 20
Herbaceous Sandbank Vegetation	1	Extremely Low	Moderate		10 to 15
River, Lake	0	No Vulnerability	Low		5 to 10
Ocean	0	No Vulnerability	Extremely low		0 to 5

Table 1: Set of classes and assigned values of hazard, vulnerability and risk.

4 Results

The presentation of the results was organized to reflect the methodological logic and meet the study's objectives, ensuring a sequential and coherent reading of the findings. Initially, statistical analyses of historical tide series are shown, focusing on 275 trends and extreme patterns. Next, the projected MSLR scenarios are presented, both in terms of frequency and total flooding. Finally, the flood risk map and its resulting impacts are discussed, allowing for a spatial reading of the associated risks and their implications.

4.1 Statistical analysis of tide gauge data

Statistical analysis of data from Macau and Areia Branca provided a clear and robust understanding and characterization of 280 some of the coastal processes in the region, as revealed by statistical data and interpretations, distinguishing between astronomical and non-astronomical processes in the context of the two estuaries.

The ATs of Macau (ATM) varied between 2.82 and 2.94 m (Table 2), with an average of 2.90 m and low dispersion (St. Dev = 0.031), indicating stability over time, with more sporadic maximums. In Areia Branca (ATAB), the values ranged from 3.19 to 3.40 m, with an average of 3.33 m, reflecting greater astronomical amplitude in the western sector, including more recurrent 285 maximums. For MT, the maximum values were 0.14 m in Macau (MTM) and 0.11 m in Areia Branca (MTAB), confirming



the low magnitude typical of this forcing in the Brazilian semiarid region, in addition to its episodic and irregular behavior, characteristic of this process in the tropics.

The Mann–Kendall test revealed no significant trends in almost all series, indicating a pattern of stability, except for MTAB (p = 0.042; Tau = -0.154), which showed a statistically significant downward trend. This result may indicate a gradual reduction in local meteorological influence, possibly associated with large-scale atmospheric modulation and/or limitations in data reconstruction, an important aspect to be discussed in methodological terms.

Descriptive Statistics							
Dates	Min	Max	Med	Mean	St. Dev	Var	Range
ATM	2.820	2.940	2.900	2.894	0.031	0.001	0.120
ATAB	3.190	3.400	3.330	3.318	0.052	0.003	0.210
MTM	0.032	0.141	0.070	0.070	0.018	0.000	0.109
MTAB	0.040	0.112	0.072	0.073	0.016	0.000	0.072

Mann-Kendall test							
Dates	Trend	Significant (h)	p-value	Z-Score	Tau	Var (S)	Denominator (S)
ATM	no trend	False	0.432	-0.786	-0.057	73491.333	271.093
ATAB	no trend	False	0.730	-0.346	-0.025	73914.333	271.872
MTM	no trend	False	0.935	-0.082	-0.006	60042.333	245.035
MTAB	decreasing	True	0.042	-2.032	-0.154	60042.333	245.035

Table 2: Descriptive statistics and Mann–Kendall test results for astronomical and meteorological tide series in Macau and Areia Branca. Initially, differences can be noted between the different processes in the region.

295 Inspection of the complete time series between 1940 and 2025 shows relative stability in AT and greater dispersion in MT, especially in Macau (Figure 4). The histograms confirm the concentration of values around the calculated means, while the non-exceedance probability (NEP) curves indicate percentages up to 95% below the mean, reinforcing that extreme events are rare but of high magnitude when compared to the maximum values obtained.

The expected maximums for the 20-year return period (RP20) were reasonably above the maximums of the time series. For 300 ATM, a maximum tide of 2,975 m is expected, while for ATAB, values of 3,454 m are expected. The expected values are close to those obtained in similar studies in the same area, such as those conducted by Araújo et al. (2021) and Aguiar et al. (2019).

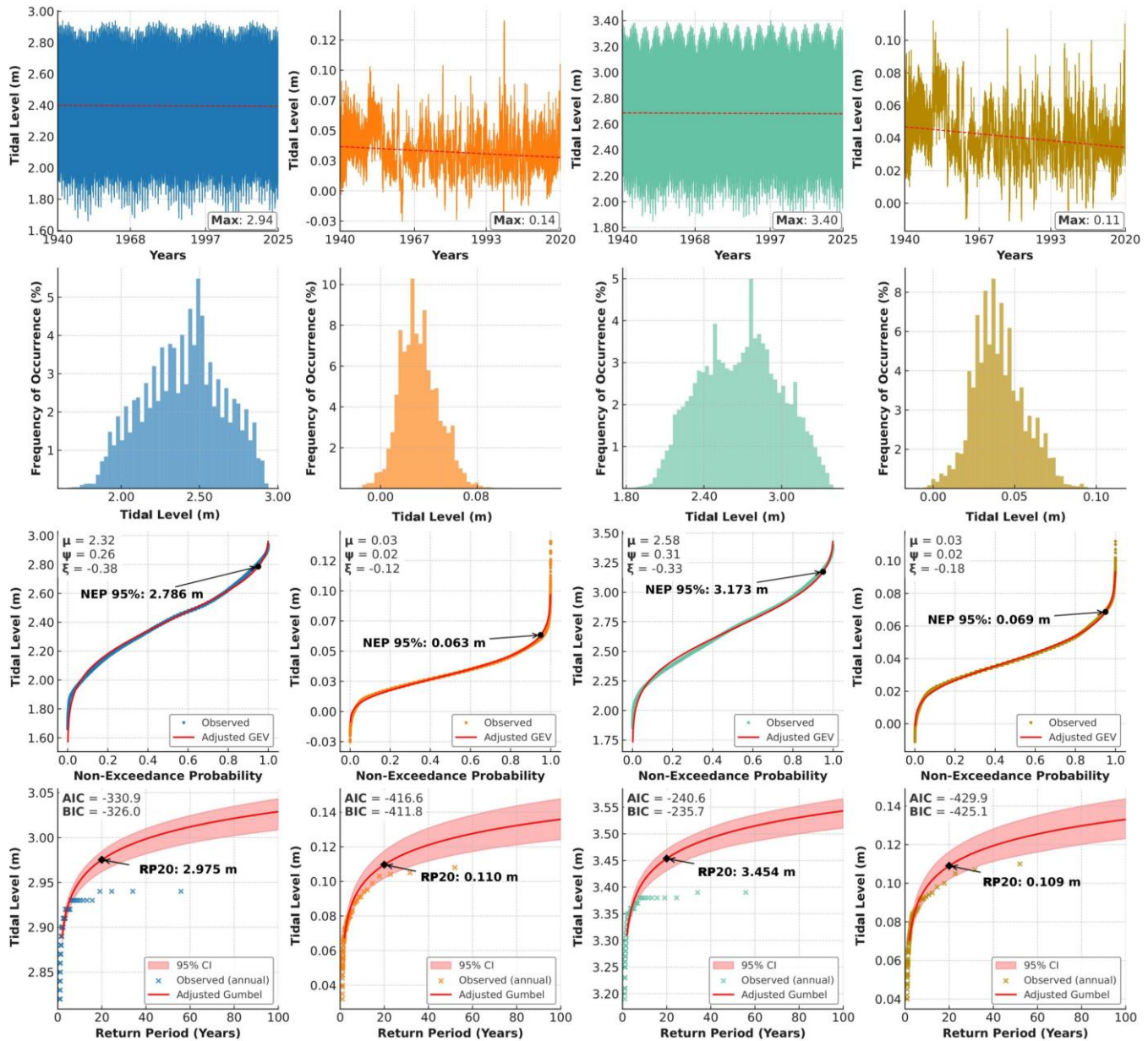
The non-astronomical effects presented quotations associated with RP20 of 0.110 m for Macau (MTM) and 0.109 m for Areia Branca (MTAB). These values are close to the 10 cm threshold already reported by Frota et al. (2016), Rodríguez et al. (2016), 305 and Melo Filho (2017) in studies on meteorological tides in Brazil and nearby regions. This convergence reinforces the methodological consistency of this work, highlighting results that are in line with the literature and supported by previous empirical bases.

The Morlet wavelet transform applied to the series of annual maximum quotas (Figure 5) revealed contrasting patterns between Macau and Areia Branca. In the ATs, it showed persistent energy on decadal scales (\approx 10 to 20 years), with low interannuality.

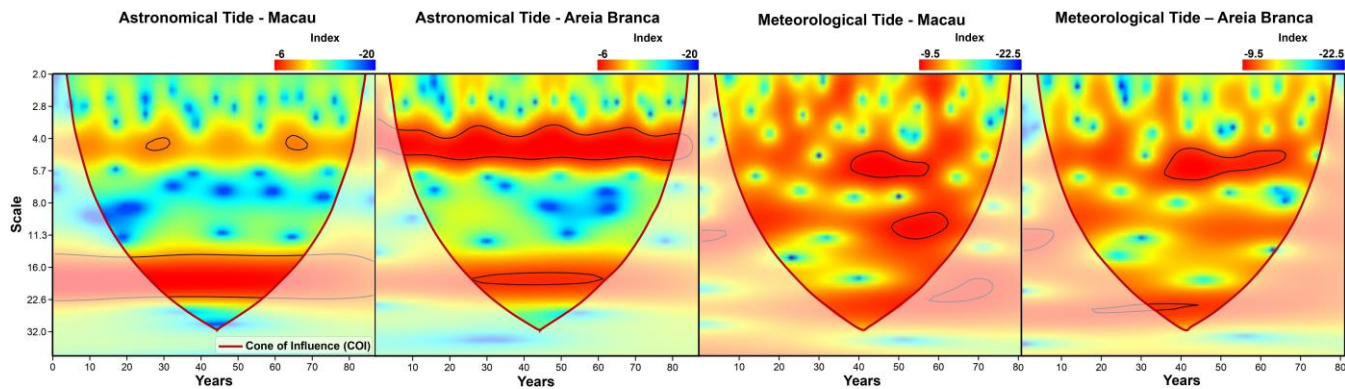
310 In Areia Branca, the energy is predominantly short interannual (\approx 3 to 6 years) and less pronounced in the long periodicity



bands. In a joint analysis of the data, the ATM is more susceptible to decadal oscillations that can potentiate extreme events when combined with atmospheric forcings.



315 **Figure 4:** Time series, frequency distributions, non-exceedance probability curves, and return period estimates of maximum astronomical and meteorological tides at Macau and Areia Branca. Prepared by the authors (2025).



320 **Figure 5: Continuous spectral analysis (Morlet wavelet) applied to maximum tide series. The Cone of Influence (COI) is indicated by the red line limiting the reliable region of the analysis. The black line indicates the significance level $p = 0.05$. The vertical axis (Scale) shows the temporal decomposition: short cycles (2–4 years, high frequency) are concentrated at the top, while long oscillations (16–32 years, low frequency) are located at the bottom. Prepared by the authors (2025).**

325 In a general analysis, ATs showed persistent energy in interannual and decadal bands, confirming their forced and predictable nature. Macau has a higher occurrence of energetic extremes in interdecadal cycles, while Areia Branca has more energetic interannual cycles.

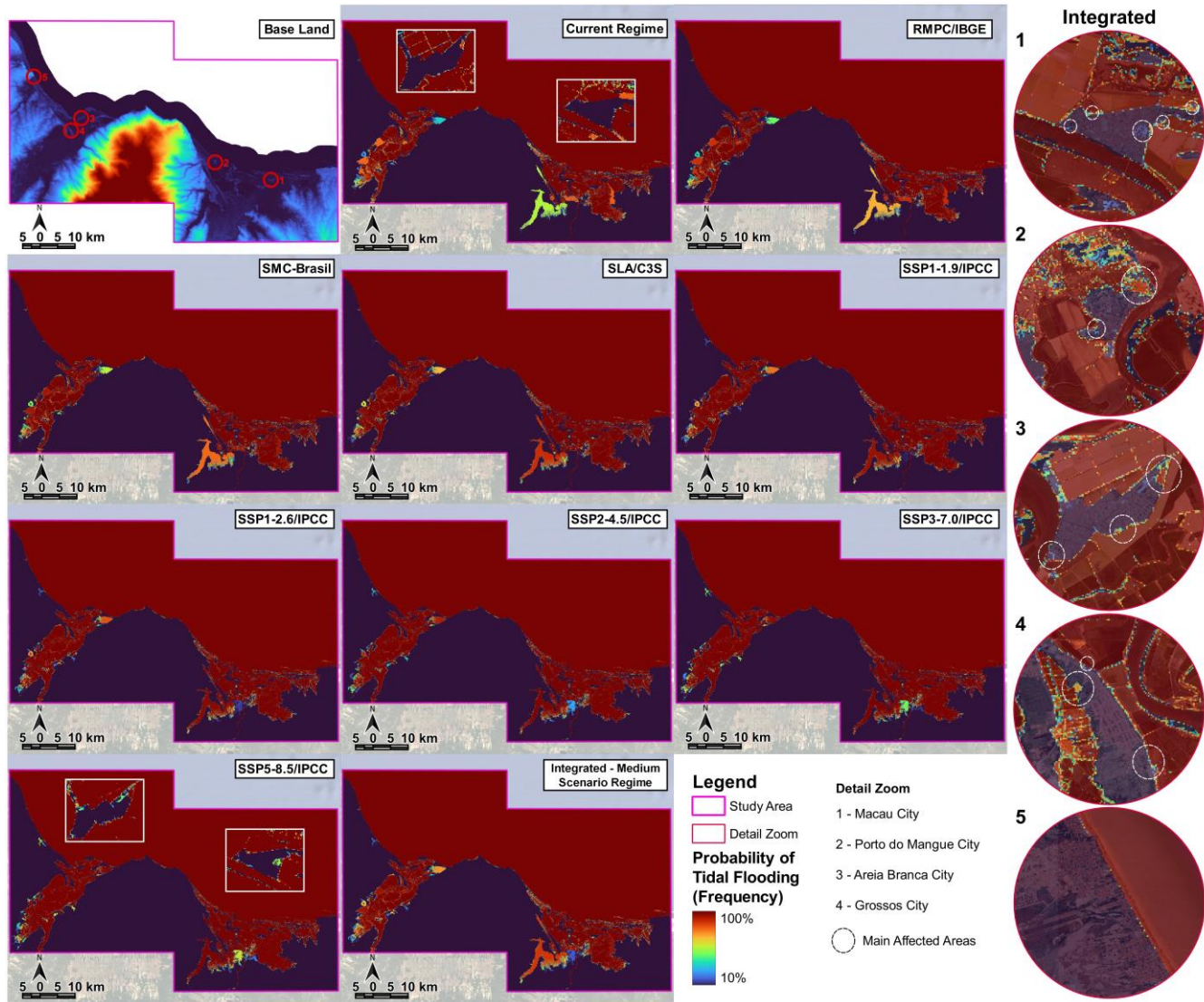
330 In MTs, the signals are more irregular, without a clear cyclicity. In Macau, the energy is episodic with irregular annual peaks (≈ 4 to 6 years), with irregular occurrences in ≈ 8 to 10 years, but without robustness. In Areia Branca, there is greater persistence in concerted annual cycles of ≈ 4 to 8 years and significant recurrence close to ≈ 20 years, suggesting modulation by regional-scale climate variability. However, it is important to note that the smoothing nature of the data tends to underrepresent actual meteorological peaks, smoothing out energy extremes, as stated by the creators of the base data (Yang et al., 2025).

The combination of AT and MT in years of higher interannual/interdecadal energy can combine energies and generate a mixed effect, intensifying potential extremes. Even though events combining meteorological and astronomical maxima are quite peculiar.

335 The AT quotas validated in the Brazilian Geodetic System (SGB), marked by the reduction level quotas (Macau: -1.1129 m; Areia Branca: -1.3532 m), allowed the RP20 quotas of 1,862 m for Macau and 2,101 m for Areia Branca to be obtained. The values found are slightly similar to the maximum elevations obtained from the Global Ocean Tides (GOT) and GOS data from SMC-Brazil, found by Silva et al (2025), which estimates a maximum regime close to 2 meters for medial portions of the area. Obtaining quotas is essential for weighing up the proposed coastal process packages.

340 **3.2 MSLR scenario modeling**

The different MSLR scenarios presented virtually similar patterns, varying essentially in the intensity of flooding, which changes significantly across the multiple scenarios (Figure 6), increasing the potential for stacking of projected daily levels in low-lying areas, progressively increasing the probability of hazards in the time frame.



345 **Figure 6: Probability scenarios for flood hazard events obtained through frequency modeling. Each plot represents a modeled scenario, with the natural terrain quadrant representing the baseline scenario used for modeling. The side portion shows a zoom-in view of only the main urban agglomerations in the study area. Map prepared by the authors (2025) using basemap data from Bing Maps (© Microsoft).**

350 In the projected frequency scenarios, the salt flats and their operational structures were considerably affected, with up to 100% of days flooded in almost all projections, a fact already expected due to the nature of the activity. However, based on SSP1-1.9, the dikes that surround the ponds (Figure 7A) were observed to overlap with a 100% probability of continuous flooding, which represents a critical point, as these dikes control the internal levels of the salt pans and estuaries, where their imbalance can cause occasional flooding due to decompression or even flash floods, a process not captured by the model but which is 355 recurrent in the region (Figure 7B).



Urban areas, in turn, showed a low probability of flooding under the current regime, restricted to a few localized features in the center of Macau and Areia Branca, but quite sporadic. However, in progressively more severe scenarios such as SSP5-8.5, these sectors will experience probabilities of 60% to 70% of flooded days by 2100 in occupied areas, respectively.



360

Figure 7: Flood relations. A - Aerial image of downtown Grossos, showing the dikes that control the levels of salt flats on the outskirts of the urban area. B - News report on a collapsed dike in Grossos in 2024. Panel A photograph by the authors (2025). Panel B adapted from Mossoró Hoje (2024), © Mossoró Hoje.

The integrated analysis, based on the average of all scenarios, shows that critical flooding points are concentrated in the main 365 urban areas of Areia Branca, Macau, and Porto do Mangue, which have a probability of flooding ranging from 60% to 80% of days in at least three occupied sectors. This condition is particularly relevant, as it suggests that maximum daily levels would already be sufficient to impact urban areas in at least six simulated scenarios. In contrast, cities such as Tibau and Grossos showed resilience even in pessimistic scenarios, with very low daily flooding, indicating that their hazard to marine intrusion remains limited.

370 In the context of a maximum event, total flooding was estimated based on sea level projection values linked to the geodetic plane for 2100 (Table 3). In a comparison between the river mouths, different behaviors were observed: in the Piranhas-Açu River, there is lateralization of the water surface in all scenarios (Figure 8), while in the Apodi-Mossoró River, the advance is internalized, revealing distinct flooding patterns conditioned by topography and river dynamics. Considering the total area, an overlap of 14% of the analysis area (about 730 km²) was obtained, which could reach 16% (849 km²) in the most pessimistic scenario.

375 On a detailed scale, Figure 9 shows the direct overlap on urban areas already under the current regime, especially in Areia Branca and Porto do Mangue. Recent occupations were observed in subdivisions and official roads located in areas of recurrent flooding, confirmed by field checks. Although other cities have proven relatively resistant in the initial scenarios, SMC-Brasil



380 trends indicate progressive intensification, with significant damage in Macau and isolated occurrences in Grossos, becoming even more critical in the most extreme IPCC scenario (2022).

Macau domain – RL: -1,1129 m						
Scenarios	Projection	ATtr20	ATrp20 (BGS)	NAErp20	RMSE	FL
Present	-	2,975	1,862	0,110	0,612	2,584
RMPG IBGE	0,104	2,975	1,862	0,110	0,612	2,688
SMC-Brasil Trend	0,193	2,975	1,862	0,110	0,612	2,777
SLA	0,309	2,975	1,862	0,110	0,612	2,893
IPCC SSP1-1.9	0,409	2,975	1,862	0,110	0,612	2,993
IPCC SSP1-2.6	0,460	2,975	1,862	0,110	0,612	3,044
IPCC SSP2-4.5	0,593	2,975	1,862	0,110	0,612	3,177
IPCC SSP3-7.0	0,716	2,975	1,862	0,110	0,612	3,300
IPCC SSP5-8.5.	0,800	2,975	1,862	0,110	0,612	3,384
Areia Branca domain – RL: -1,3532 m						
Scenarios	Projection	ATtr20	ATrp20 (BGS)	NAErp20	RMSE	FL
Present	-	3,454	2,101	0,109	0,612	2,822
RMPG IBGE	0,104	3,454	2,101	0,109	0,612	2,926
SMC-Brasil Trend	0,193	3,454	2,101	0,109	0,612	3,015
SLA	0,309	3,454	2,101	0,109	0,612	3,130
IPCC SSP1-1.9	0,409	3,454	2,101	0,109	0,612	3,231
IPCC SSP1-2.6	0,460	3,454	2,101	0,109	0,612	3,282
IPCC SSP2-4.5	0,593	3,454	2,101	0,109	0,612	3,415
IPCC SSP3-7.0	0,716	3,454	2,101	0,109	0,612	3,538
IPCC SSP5-8.5.	0,800	3,454	2,101	0,109	0,612	3,622

Table 3: Projected flood levels linked to the geodetic reference plane. ATrp20 corresponds to the astronomical tide projected for a 20-year return period, while ATrp20 (BGS) represents the same level adjusted and validated on the geodetic plane. NAErp20 refers to the meteorological tide projected for the same return period. The RMSE expresses the average error of the digital elevation model used as a basis, and FL corresponds to the final flood elevation resulting from the combination of these parameters.

385

In the segmentation by hazard classes, 731 km² were identified as being at extremely high risk, corresponding to 14% of the study area. The urban areas of Areia Branca and Porto do Mangue stood out as the most affected, with about 10% of the urban grid compromised, with the city of Areia Branca being the most impacted with 0.21 km² (Table 4). Macau and Grossos 390 presented specific areas of extreme hazard, affecting only specific infrastructure sectors. Tibau was the only less vulnerable city, with less than 1% overlap, reinforcing its lower exposure to climate risk. Locations such as Upanema beach and Povoado Cristovão (Areia Branca), Povoado Rosado (Porto do Mangue), and Ilha de Santana village (Macau) also presented critical areas, but less than the urban centers listed.

The patterns identified corroborate previous findings, such as in Grossos, where the results confirm less intense projections, 395 but spatially similar to those of Silva et al. (2024). In Macau, the overlap was lower than that observed by Araújo et al. (2021), but occurred in the same low-lying urban areas. In Areia Branca, the affected areas coincided exactly with those evidenced by Aguiar et al. (2019). In Tibau, low exposure confirmed the resilience delimited by Rabelo et al. (2023) when analyzing conservation areas near the municipality. These parallels reinforce the consistency of the results and the validity of the mapping in identifying endemic areas of hazard.



400

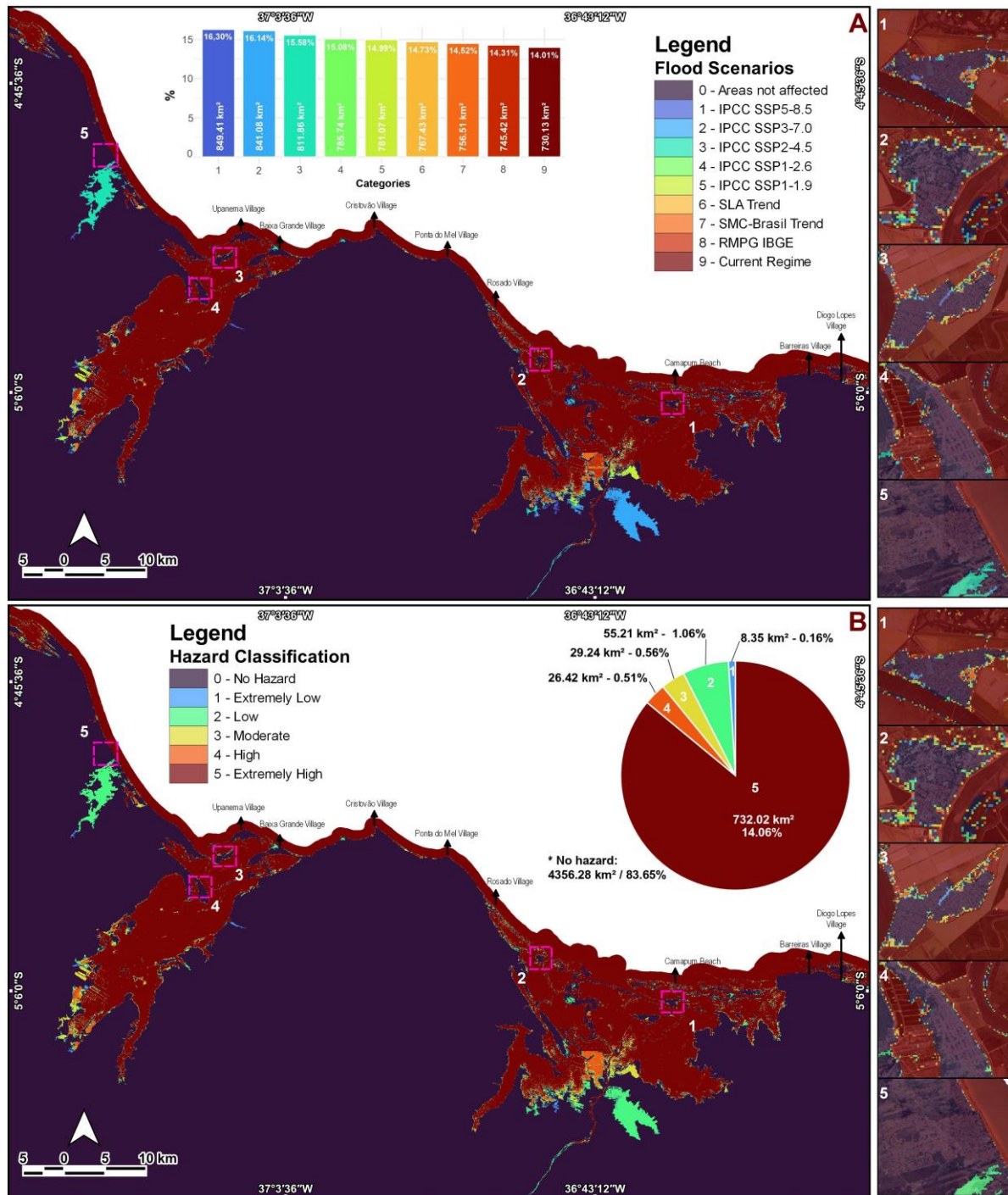


Figure 8: Classification of MSLR scenarios in the study area (A) and classification of tidal flooding hazards (B) by sector. The far-right column shows the scale zones in the cities of the study area. The graphs on the maps indicate the percentages of the total area occupied. Map prepared by the authors (2025) using basemap data from Bing Maps (© Microsoft).

405



Figure 9: Photographic records of the main areas indicated by the model as extremely high risk. It is noteworthy to observe the lowering of the mapped areas, especially Areia Branca, where flooding was verified in the field; A - section of the urban area of Macau with the most susceptible area; B - section of the urban area of Porto do Mangue with a low-lying portion prone to flooding; C - urban area of Areia Branca with flooding boundaries; and D - urban area of Grossos with channels prone to overflowing. Photographs by the authors (2025).

410

Urban Area	Urban Area (km ²)	Flood Area (km ²)	Flood (%)
Porto do Mangue	0,732	0,080	10,884
Macau	1,530	0,023	1,489
Areia Branca	2,052	0,211	10,278
Grossos	1,449	0,039	2,677
Tibau	4,523	0,030	0,545

Table 4: Percentage of major urban areas at extreme risk of tidal flooding.



4.3 Risk of tidal flooding

The validated land use showed the predominance of savanna formations, which correspond to Caatinga environments, occupying a total area of 47% (Figure 10) in relation to the study area. Next, pasture areas (13%) and mosaics of diverse uses (14%) stand out, comprising the second and third groups. Among specific uses, salt pans, the main activity in the region, deserve mention, representing 7% of the area, as do urban areas, which total 2%.

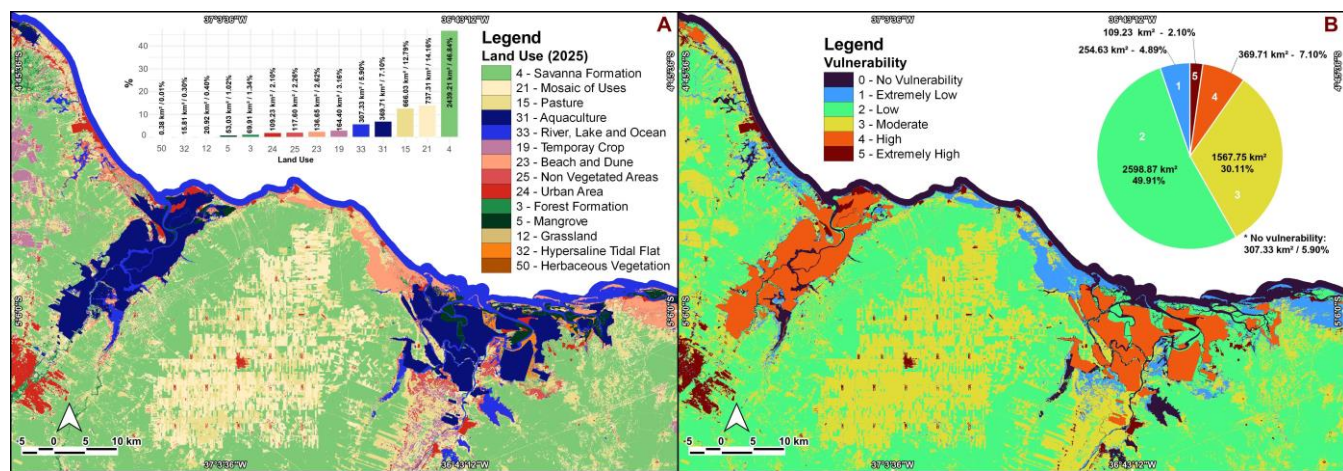


Figure 10: Land use in the study area (A) and vulnerability classification (B). The graphs at the top indicate the percentages of areas occupied by each class. Map prepared by the authors (2025) using data from Mabpiomas (2025).

With regard to vulnerability, the sectorization indicated 478.94 km² classified as high and extremely high vulnerability, equivalent to 9.20% of the area. In contrast, most of the territory (60.70%) was classified as low to no vulnerability, revealing a strong spatial contrast between high-risk zones and more stable areas.

The combination of the results of the hazard and vulnerability mapping resulted in the final tidal flood risk map. The spatialized risk classes showed largely predictable patterns, considering the previous analyses. The high risk class stands out, corresponding to 6.37% of the total area, while the extremely high risk category, although small (0.04% overall), was concentrated in critical areas, especially in urban sectors of the cities of Porto do Mangue, Macau, Areia Branca, and Grossos, in addition to communities such as Ponta do Mel, Rosado, Diogo Lopes, and Upanema, with considerable percentages, especially the villages of Baixa Grande in Areia Branca, Ilha de Santana in Macau, and Barra in Grossos, which had percentages of affected urban areas close to 20% (Table 5).

The spatial distribution of risk areas can be seen in Figure 11, the areas of very high flooding closely resemble the findings of Borri et al. (2012) in Areia Branca. In addition, occurrences were identified in most of the villages, extending beyond urban limits and highlighting the vulnerability of coastal communities in the region. This pattern broadens the interpretation of the data beyond urban centers, reinforcing the diffuse nature of the risk associated with tidal flooding. These communities are mostly traditional fishing communities that play an important social and economic role in the region.



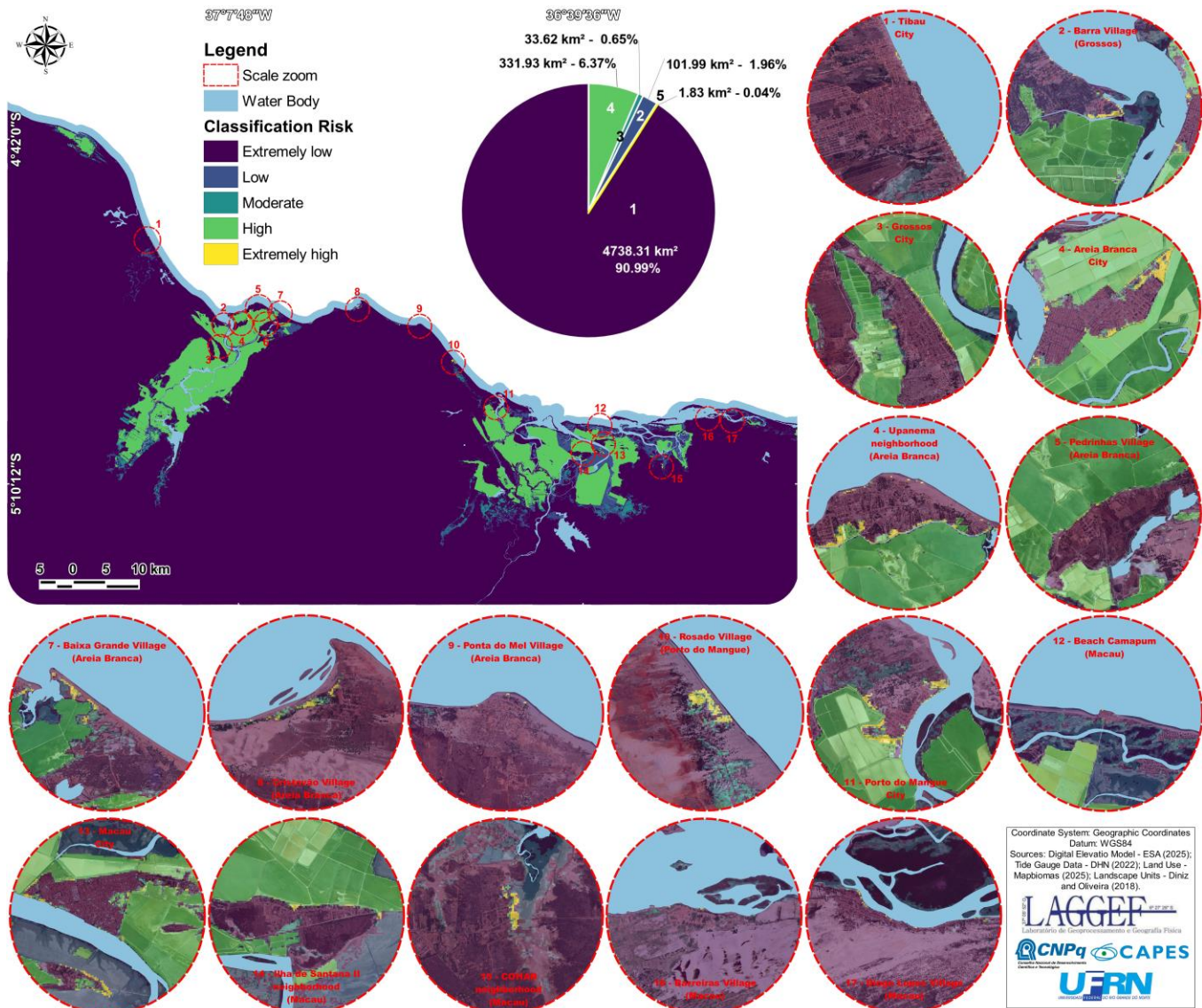
Locations	Area	Extremely Low		Low		Moderate		High		Extremely High	
Cities and districts	Total	Area	%	Area	%	Area	%	Area	%	Area	%
<u>*Macau (Urban Center)</u>	1.530	1.310	86%	0.056	4%	0.060	4%	0.064	4%	0.041	3%
Camapum Beach (Macau)	0.030	0.028	94%	0.002	6%	-	-	-	-	-	-
COHAB neighborhood (Macau)	0.412	0.363	88%	0.009	2%	0.010	3%	0.006	1%	0.024	6%
Ilha de Santana Village (Macau)	0.280	0.145	52%	0.026	9%	0.021	7%	0.043	15%	0.045	16%
Ilha de Santana II Village (Macau)	0.813	0.713	88%	0.022	3%	0.049	6%	0.010	1%	0.019	2%
Barreiras Village (Macau)	0.478	0.476	100%	-	-	-	-	-	-	-	-
Diogo Lopes Village (Macau)	0.734	0.702	96%	0.009	1%	0.012	2%	0.001	0%	0.009	1%
<u>*Areia Branca (Urban Center)</u>	2.052	1.621	79%	0.090	4%	0.120	6%	0.067	3%	0.154	8%
Upanema Beach (Areia Branca)	2.648	2.408	91%	0.029	1%	0.034	1%	0.027	1%	0.150	6%
Baixa Grande Village (Areia Branca)	0.235	0.166	71%	0.014	6%	0.010	4%	0.007	3%	0.037	16%
Pedrinhas Village (Areia Branca)	0.353	0.336	95%	0.009	2%	0.002	1%	0.003	1%	0.004	1%
Cristóvão Village (Areia Branca)	1.274	1.163	91%	0.024	2%	0.027	2%	0.019	1%	0.041	3%
Ponta do Mel Village (Areia Branca)	0.489	0.485	100%	-	-	-	-	-	-	-	-
<u>*Porto do Mangue (Urban Center)</u>	0.728	0.449	62%	0.048	7%	0.045	6%	0.035	5%	0.150	21%
Rosado Village (Porto do Mangue)	0.526	0.280	53%	0.040	8%	0.075	14%	0.012	2%	0.119	23%
<u>*Grossos (Urban Center)</u>	1.449	1.376	95%	0.026	2%	0.017	1%	0.008	1%	0.023	2%
Barra Village (Grossos)	0.193	0.135	70%	0.008	4%	0.006	3%	0.001	0%	0.043	23%
<u>*Tibau (Urban Center)</u>	4.523	4.479	99%	0.023	1%	-	-	-	-	-	-

Table 5: Risk percentages defined in cities and towns. The underlined sections indicate the urban centers of cities.

The results obtained allow for overlap with urban real estate data, aiming to observe what these extremely high-risk zones section and where they are located, given that although the locations are delimited, they do not always coincide with effectively occupied areas, including vacant land and public infrastructure.

440 By superimposing the risk map generated with municipal real estate databases, it was possible to identify residential areas and land that could potentially be affected, enabling estimates of potential financial and area damage (Figure 12). Several areas can be seen overlapping the risk zone, but few have a high density of residences. In particular, the cities of Areia Branca, Porto 445 do Mangue, and Macau had significant concentrations of residences that could be affected, as did the villages of Barra, Cristóvão, the COHAB neighborhood, and the village of Baixa Grande, with significant overlaps.

The potential flooding represents the loss of approximately 123,000 m² of built area out of a total of 574,000 m² (Table 5), which in practice means flooding with the potential for significant material losses, understood as concrete damage to built or 450 unbuilt property. In terms of structural damage to homes, the quantification of damage was estimated at around R\$ 36 million, equivalent to US\$ 6 million, with general damage to land of approximately R\$ 158 million, US\$ 29 million, representing a worrying threshold for small municipalities with low response capacity. The main highlight is Areia Branca, which concentrated the highest projected losses, with R\$ 13 million in financial damage to built-up areas, as a result of its higher urban density in exposed areas.



455 **Figure 11:** spatialization of quantified risks for the study area and surrounding area, on a general scale and in detail, for cities and villages. Map prepared by the authors (2025) using basemap data from Bing Maps (© Microsoft).

The modeling carried out, in general, with the projection of future scenarios and the identification of financial damages, demonstrates the urgency of adaptive and mitigating measures, since even with impacts localized at the regional level, the 460 outbreak of a potentially destructive event can seriously compromise the environmental and socioeconomic stability of coastal municipalities, directly affecting the quality of life of the population. The scale of the estimated damage makes it clear that addressing coastal climate risk requires prior planning and institutional mobilization, under penalty of irreversible losses.



Figure 12: Spatial distribution of risk areas and their relationship with residences in urban areas and villages. Map prepared by the authors (2025) using basemap data from Bing Maps (© Microsoft).

465

Location	Homes Affected	Lands Affected	Damaged Area (Homes)	Damaged Area (Land)	% Damage (Homes)	% Damage (Land)	Price/m ²	Losses (Homes)	Losses (Land)
Grossos	15	33	994	9620.397	34%	26%	120	R\$ 119,272.21	R\$ 1,154,447.68
Barra	40	43	5812	18966.35	94%	82%	170	R\$ 988,062.50	R\$ 3,224,279.25
Porto do Mangue	116	178	9363	82702.38	74%	66%	220	R\$ 2,059,765.54	R\$ 18,194,522.65
Rosado	35	46	4405	40831.85	82%	72%	200	R\$ 880,955.84	R\$ 8,166,369.33
Macau	165	199	27321	87332.40	72%	67%	400	R\$ 10,928,251.89	R\$ 34,932,959.48
Ilha de Santana I	184	257	15827	50078.76	77%	75%	60	R\$ 949,624.01	R\$ 3,004,725.75
Ilha de Santana II	8	25	299	16944.94	62%	48%	50	R\$ 14,949.03	R\$ 847,247.14
COHAB	23	36	1601	10473.78	92%	87%	100	R\$ 160,065.47	R\$ 1,047,378.20
Barreiras	13	13	1290	1993.81	94%	94%	147	R\$ 189,615.98	R\$ 293,089.82
Diogo Lopes	35	39	1295	2115.17	45%	37%	150	R\$ 194,312.21	R\$ 317,275.31
Areia Branca	215	304	30742	109244.28	72%	71%	450	R\$ 13,834,003.18	R\$ 49,159,924.79
Upanema	63	119	7538	54941.56	65%	51%	280	R\$ 2,110,632.14	R\$ 15,383,636.90
Baixa Grande	51	78	9941	34758.68	70%	69%	200	R\$ 1,988,266.33	R\$ 6,951,735.26
Cristovão	35	67	5803	52054.79	85%	64%	300	R\$ 1,740,994.68	R\$ 15,616,437.85
Ponta do Mel	4	7	692	1367.85	99%	61%	220	R\$ 152,221.66	R\$ 300,928.00
Pedrinhas	6	13	164	1034.98	38%	38%	100	R\$ 16,388.27	R\$ 103,497.87
Total	1,008	1,457	123087	574461.97	72%	63%	-	R\$ 36,327,380.93	R\$ 158,698,455.28

Figure 13: Quantification of Affected Areas, Percentage of Damage, and Economic Losses (Homes and Land) by Location. For the villages of Rosado, Barra, Ponta do Mel, Pedrinhas, and the COHAB neighborhood, estimates were made by interpolation because they had few or no data samples.



5 Discussion

470 The analyses showed that tidal flooding risks are mainly concentrated in the urban areas of Areia Branca, Macau, and Porto do Mangue, with field validations of sections that are already susceptible under the current regime. The integrated damage estimate pointed to significant structural losses, reaching approximately R\$ 36 million in buildings and R\$ 158 million in land. In addition, a potential flooding event would directly compromise the salt production activity strategically concentrated in the rural area and main economic base of these municipalities, which would potentially amplify the impacts. Areia Branca stands 475 out as the municipality most affected in terms of built-up areas. These figures confirm the hypothesis that, even in conservative scenarios, the financial and social impacts tend to be significant and spatially concentrated.

480 The combination of low topography and recurring maximum astronomical levels reinforced critical flooding patterns. In severe scenarios, there was an increase in the frequency of flooded days in already occupied areas, as well as an increase in maximum levels, which increased urban exposure. Interannual and decadal processes add variability, and the coincidence of astronomical and meteorological extremes, although rare, can potentiate critical events. This reading reinforces the notion that coastal risks in the Semi-Arid Coast are not limited to the trend of sea level rise, but result from a combination of multiple hydrodynamic factors.

485 The results obtained corroborate previous mappings in the region: in Areia Branca, areas coinciding with those of Aguiar et al. (2019) were identified; in Macau, patterns similar to those of Araújo et al. (2021) were found, albeit with different magnitudes; in Tibau, low exposure was comparable to that of Rabelo et al. (2023); and in Grossos, less intense but spatially consistent projections confirm the findings of Silva et al. (2024). This bibliographic convergence indicates the spatial robustness of the method and strengthens its regional applicability. The difference here lies in integrating physical risk with localized economic losses, offering a useful comparative framework for decision-making, using tools and techniques with very low aggregate costs.

490 The recurrence of flooding in the region reinforces the natural susceptibility of the cities studied, many of which are located in low-lying areas on estuarine islands. These naturally flood-prone areas have already suffered significant impacts in the past, as in the case of Macau, whose current urban center is the result of relocation after its old center was submerged, swallowed by the tides in the 19th century (Araújo, 2020; IBGE, 2025). This history shows that floods are not unprecedented phenomena, but rather recurring events, and that their effects will be exacerbated by projected MSLR scenarios. In the short term, strict 495 control of saltpan dikes tends to mitigate more frequent flooding, but remains limited in the face of extreme events, which, according to projections, will tend to become more recurrent, posing new challenges for urban adaptation and territorial management.

500 From a conceptual point of view, the findings reinforce probabilistic approaches to coastal risk that weigh frequency and maximum events within a validated geodetic framework. Risk maps and their readings are tools for territorial screening and strategic mobilization, supporting priority measures such as coastal protection and management, land use guidelines in low-



lying areas, and urban contingency plans. Although limited by 30 m resolution and vertical uncertainties, the products are methodologically consistent and practical, fulfilling their role as a starting point for public policy.

It should be noted, however, that the results should be interpreted as a reference for regional hydrodynamic trends, not as exact representations of reality, even though some results have successfully represented actual processes. Interpretations should be
505 considered with caution, especially due to the limitations imposed by the 30-meter spatial resolution of the DEM, the inherent simplification of the model used, which does not consider lateral processes and tidal damping, and the interpolation of real estate data in settlements with an incipient market, facts that naturally impose considerable margins of error. Nevertheless, by demonstrating that open data allows for consistent and auditable analyses, with real-world validations in the field, the study advances the central hypothesis that it is possible to project regional MSLR scenarios and identify endemic risk areas with
510 strong applied value.

Looking ahead, it is recommended that new models be constructed for the area at the local level, using DEMs with greater accuracy and resolution to capture microtopography, complete real estate databases, and periodic field campaigns to refine hotspots. It would also be very valuable to adopt a methodology that incorporates the combined effect, covering not only coastal flooding (by tides) but also its interaction with river flooding events from the two main rivers in the study area.

515 Explicit trends for advancing research in the region should move toward integrating more sophisticated dynamic modeling with updated socioeconomic data, allowing for a better understanding of the interaction between hydrodynamic processes and social vulnerabilities. Overall, the advances made in this study point to an alarming scenario: all the municipalities analyzed are vulnerable to climate change and at high or extremely high risk of flooding, which contrasts with their low financial capacity to address the risks associated with MSLR, reinforcing the urgency of climate adaptation plans to protect coastal
520 communities and their critical infrastructure.

The cities in the region were historically built on slightly higher ground, serving as a real front line against imminent flooding. However, part of their urban areas and land remains in extremely high-risk zones, as do the solar salt flats, the main local economic activity. This is one of the lowest-lying coasts on the planet, where salt pan dikes could play a strategic role in containing flooding events in the near future. However, this planning needs to be refined through coordination between public
525 authorities and the salt industry in order to ensure greater territorial and economic resilience.

6 Conclusions

In summary, the main findings indicate a concentration of coastal risk in low-lying urban areas and salt flats, with occasional validation in the field, and significant potential economic losses across the region, particularly in Areia Branca. The probabilistic approach adopted, anchored in the geodetic plane and free data, provides a comparable and actionable regional
530 framework for adaptive planning, even recognizing the vertical uncertainty and hydrodynamic simplification of the model. Thus, the data and insights obtained by the study suggest that adaptation policies focused on land use planning and response plans in already susceptible sectors can reduce future losses and, to a certain extent, facilitate climate change mitigation.



The methodology has proven to be effective and easy to replicate, allowing for dynamic risk and loss assessment at low cost, provided that there is skilled labor available for the operation. It is especially useful in regions where climate change mitigation
535 strategies are lacking, offering quick and consistent support for mobilizing coastal adaptation policies.

Regarding the prospects for this work, it is important to mention that, in order to make progress, it is crucial to conduct new studies to develop robust models; invest in real-time tide gauge data collection systems and systematic geodetic validations in the field, keeping in mind the logic of iteration: models generate hypotheses; the field confirms/adjusts them, and new rounds refine the risk on a fine scale. These processes contribute to the generation of increasingly accurate data, which is extremely
540 useful in addressing climate change.

Acknowledgments

The authors are grateful for the financial support provided by the National Council for Scientific and Technological Development (CNPq) and the Coordination for the Improvement of Higher Education Personnel (CAPES – Funding Code 001). The authors also thank the Graduate Program in Geography at the Federal University of Rio Grande do Norte (UFRN)
545 for its organizational support, which provided essential academic and institutional support for the completion of this study.

Author contribution

TCLS and MTMD designed the study. TCLS, JPS, and PVNA acquired the geodetic data. TCLS processed the data. MTMD and PVNA performed the final data verification. BF and JYGS made the final adjustments to the study. All authors reviewed this article.

550 References

Aguiar, L. S., Amaro, V. E., Araújo, P. V. N., and Santos, A. L. S.: Low cost geotechnology applied to flood risk assessment in coastal urban areas in climate change scenarios, *Anuário Inst. Geociênc.*, 42, 267–290, https://doi.org/10.11137/2019_1_267_290, 2019.

Ahmed, T., Creedon, L., and Gharbia, S.: Low-cost sensors for monitoring coastal climate hazards: a systematic review and
555 meta-analysis, *Sensors*, 23, 1717, <https://doi.org/10.3390/s23031717>, 2023.

Almaliki, A. H., Zerouali, B., Santos Silva, A. A., Sherif, , and Ali, E.: Assessing coastal vulnerability and land use to sea level rise in Jeddah province, Kingdom of Saudi Arabia, *Heliyon*, 9, e18508, <https://doi.org/10.1016/j.heliyon.2023.e18508>, 2023.

Anderson, T. R., Fletcher, C. H., Barbee, M. M., Romine, B. M., Lemmo, S., and Delevaux, J. M. S.: Modeling multiple sea level rise stresses reveals up to twice the land at risk compared to strictly passive flooding methods, *Sci. Rep.*, 8, 1,
560 <https://doi.org/10.1038/s41598-018-32658-x>, 2018.



Antonioli, F., De Falco, G., Lo Presti, V., Moretti, L., Scardino, G., Anzidei, M., Bonaldo, D., Carniel, S., Leoni, G., Furlani, S., et al.: Relative sea-level rise and potential submersion risk by 2100 in 16 Mediterranean coastal plains, *Water*, 12, 2173, <https://doi.org/10.3390/w12082173>, 2020.

565 Araújo, P. V. N.: Geotecnologias de alta precisão no mapeamento de georisco a inundações frente às mudanças climáticas, PhD thesis, Universidade Federal do Rio Grande do Norte, Natal, 157 pp., 2020.

Araújo, P. V. N., Amaro, V. E., Alcoforado, A. V. C., and Santos, A. L. S.: Vertical accuracy and calibration of digital elevation models (DEMs) for the Piranhas-Assu River Basin, Rio Grande do Norte, *Anuário Inst. Geociênc.*, 41, 351–364, https://doi.org/10.11137/2018_1_351_364, 2019.

570 Araújo, V. N., Amaro, V. E., Aguiar, L. S., Lima, C. C., and Lopes, A. B.: Tidal flood area mapping in the face of climate change scenarios: case study in a tropical estuary in the Brazilian semi-arid region, *Nat. Hazards Earth Syst. Sci.*, 21, 3353–3366, <https://doi.org/10.5194/nhess-21-3353-2021>, 2021.

Arnell, N. W., Lowe, J. A., Bernie, D., Nicholls, R. J., Brown, S., Challinor, A. J., and Osborn, T. J.: The global and regional impacts of climate change under representative concentration pathway forcings and shared socioeconomic pathway scenarios, *Environ. Res. Lett.*, 14, 084046, <https://doi.org/10.1088/1748-9326/ab35a6>, 2019.

575 Barbosa, M. A., Boski, T., Bezerra, F. H. R., Lima-Filho, F. P., Gomes, M. P., Pereira, L., and Maia, R. P.: Late Quaternary infilling of the Assu River embayment and related sea level changes in NE Brazil, *Mar. Geol.*, 405, 23–37, <https://doi.org/10.1016/j.margeo.2018.07.014>, 2018.

Becker, M., Karpytchev, M., and Hu, A.: Increased exposure of coastal cities to sea-level rise due to internal climate variability, *Nat. Clim. Change*, <https://doi.org/10.1038/s41558-023-01603-w>, 2023.

580 Blaikie, P., Cannon, T., Davis, I., and Wisner, B.: *At risk: natural hazards, people's vulnerability and disasters*, Routledge, London, 1994.

Boehnke, R. F., Hoppe, T., Brezet, H., and Blok, K.: Good practices in local climate mitigation action by small and medium-sized cities; exploring meaning, implementation and linkage to actual lowering of carbon emissions in thirteen municipalities in The Netherlands, *J. Clean. Prod.*, 207, 630–644, <https://doi.org/10.1016/j.jclepro.2018.09.264>, 2019.

585 Boori, M. S., Amaro, V. E., and Targino, A.: Coastal risk assessment and adaptation of the impact of sea-level rise, climate change and hazards: a RS and GIS based approach in Apodi-Mossoró estuary, Northeast Brazil, *Int. J. Geomatics Geosci.*, 2, 815–832, https://www.academia.edu/download/48334525/Coastal_risk_assessment_and_adaptation_o20160826-2730-1d66a70.pdf, 2012.

Bricongne, J.-C., Meunier, B., and Pouget, S.: Web-scraping housing prices in real-time: the Covid-19 crisis in the UK, *J. Hous. Econ.*, 59, 101906, <https://doi.org/10.1016/j.jhe.2022.101906>, 2022.

Busman, D. V., Amaro, V. E., and Souza-Filho, P. W. M.: Análise estatística multivariada de métodos de vulnerabilidade física em zonas costeiras tropicais, *Rev. Bras. Geomorfol.*, 17, 499–516, <https://doi.org/10.20502/rbg.v17i3.912>, 2016.

Cabana, D., Rölfer, L., Evadzi, P., and Celliers, L.: Enabling climate change adaptation in coastal systems: a systematic literature review, *Earth's Future*, 11, <https://doi.org/10.1029/2023ef003713>, 2023.



595 Cappucci, S., Carillo, A., Iacono, R., Moretti, L., Palma, M., Righini, G., Antonioli, F., and Sannino, G.: Evolution of coastal environments under inundation scenarios using an oceanographic model and remote sensing data, *Remote Sens.*, 16, 2599, <https://doi.org/10.3390/rs16142599>, 2024.

Cartwright, A., Brundrit, G., and Fairhurst, L.: Global climate change and adaptation – a sea level rise risk assessment, Phase Four: adaptation and risk mitigation measures for Cape Town, Stockholm Environment Institute, Stockholm, 600 [https://resource.capetown.gov.za/documentcentre/Documents/City%20research%20reports%20and%20review/Phase%203%20-%20A%20Sea-Level%20Rise%20Risk%20Assessment%20\(SLRRA\).pdf](https://resource.capetown.gov.za/documentcentre/Documents/City%20research%20reports%20and%20review/Phase%203%20-%20A%20Sea-Level%20Rise%20Risk%20Assessment%20(SLRRA).pdf), 2008.

Copernicus Climate Change Service (C3S): Global Ocean Gridded L4 Sea Surface Heights and Derived Variables Reprocessed, dataset SEALEVEL_GLO_PHY_CLIMATE_L4_MY_008_057, <https://doi.org/10.48670/moi-00145>, 2025.

Croteau, R., Pacheco, A., and Ferreira, Ó.: Flood vulnerability under sea level rise for a coastal community located in a 605 backbarrier environment, *Portugal, J. Coast. Conserv.*, 27, 4, <https://doi.org/10.1007/s11852-023-00955-x>, 2023.

Darsan, J., Asmath, H., and Jehu, A.: Flood-risk mapping for storm surge and tsunami at Cocos Bay (Manzanilla), Trinidad, *J. Coast. Conserv.*, 17, 679–689, <https://doi.org/10.1007/s11852-013-0276-x>, 2013.

De Lima, L. T., Fernández-Fernández, S., Weiss, C. V. C., Bitencourt, V., and Bernardes, C.: Free and open-source software for geographic information system on coastal management: a study case of sea-level rise in southern Brazil, *Reg. Stud. Mar. Sci.*, 48, 102025, <https://doi.org/10.1016/j.rsma.2021.102025>, 2021.

Déguénon, M., Adade, R., Teka, O., Aheto, D. W., and Sinsin, B.: Sea-level rise and flood mapping: a review of models for coastal management, *Nat. Hazards*, 120, 2155–2178, <https://doi.org/10.1007/s11069-023-06225-1>, 2023.

Depsky, N., Bolliger, I., Allen, D., Choi, J. H., Delgado, M., Greenstone, M., Hamidi, A., Houser, T., Kopp, R. E., and Hsiang, S.: DSCIM-Coastal v1.1: an open-source modeling platform for global impacts of sea level rise, *Geosci. Model Dev.*, 16, 615 4331–4366, <https://doi.org/10.5194/gmd-16-4331-2023>, 2023.

Diniz, M. T. M., Vasconcelos, F. P., and Martins, M. B.: Technological innovation in Brazilian sea salt production and the resulting socio-territorial changes: an analysis from the perspective of Schumpeter's theory of entrepreneurship, *Soc. Nat.*, 27, 421–437, <https://doi.org/10.1590/1982-451320150305>, 2015.

Diniz, M. T. M. and Vasconcelos, F. P.: Natural conditions for the sea salt production in Brazil, *Mercator (Fortaleza)*, 16, 620 <https://doi.org/10.4215/rm2017.e16013>, 2017.

Diniz, M. T. M. and Oliveira, G. P. de: Proposal for meso-scale compartmentalization of the Northeastern Brazilian coast, *Rev. Bras. Geomorfol.*, 17, <https://doi.org/10.20502/rbg.v17i3.844>, 2016.

Dwarakisha, G. S., Vinaya, S. A., Natesan, U., Asano, T., Kakinuma, T., Venkataramana, K., Pai, B. J., and Babita, M. K.: Coastal vulnerability assessment of the future sea level rise in Udupi coastal zone of Karnataka state, west coast of India, 625 *Ocean Coast. Manage.*, 52, 467–478, <https://doi.org/10.1016/j.ocemoaman.2009.07.007>, 2009.

Eduardo, F., Matheus, , Túlio, M., and Pereira, P.: Coastal geoheritage and sustainability: a study in the low coast of Costa Branca, Rio Grande do Norte, Brazil, *Sustainability*, 17, 6709, <https://doi.org/10.3390/su17156709>, 2025.



Eilander, D., Couasnon, A., Leijnse, T., Ikeuchi, H., Yamazaki, D., Muis, S., Dullaart, J., Haag, A., Winsemius, H. C., and Ward, P. J.: A globally applicable framework for compound flood hazard modeling, *Nat. Hazards Earth Syst. Sci.*, 23, 823–846, <https://doi.org/10.5194/nhess-23-823-2023>, 2023.

Ekeu-wei, I. T. and Blackburn, G. A.: Applications of open-access remotely sensed data for flood modelling and mapping in developing regions, *Hydrology*, 5, 39, <https://doi.org/10.3390/hydrology5030039>, 2018.

European Space Agency (ESA): Copernicus DEM GLO-30: global digital elevation model at 30-meter resolution, Copernicus Open Access Hub, <https://scihub.copernicus.eu/>, 2021.

630 635 IBGE – Banco de Dados Geodésicos (BDG): <http://www.bdg.ibge.gov.br/appbdg/>, 2025.

Feenstra, J. F.: Manual of methods for impact assessment and adaptation strategies to climate change, United Nations Environment Programme, Nairobi, <https://research.vu.nl/ws/portalfiles/portal/73664742/f1>, 1998.

Fila, D., Füngfeld, H., and Dahlmann, H.: Climate change adaptation with limited resources: adaptive capacity and action in small- and medium-sized municipalities, *Environ. Dev. Sustain.*, <https://doi.org/10.1007/s10668-023-02999-3>, 2023.

640 645 Frota, F. F., Truccolo, E. C., and Schettini, C. A. F.: Tidal and sub-tidal sea level variability at the northern shelf of the Brazilian Northeast region, *An. Acad. Bras. Ciênc.*, 88, 1371–1386, <https://doi.org/10.1590/0001-3765201620150162>, 2016.

Gesch, D. B.: Best practices for elevation-based assessments of sea-level rise and coastal flooding exposure, *Front. Earth Sci.*, 6, <https://doi.org/10.3389/feart.2018.00230>, 2018.

González-Trujillo, J. D., Román-Cuesta, R. M., Muñiz-Castillo, A. I., et al.: Multiple dimensions of extreme climate events and their impacts on biodiversity, *Clim. Change*, 176, 155, <https://doi.org/10.1007/s10584-023-03622-0>, 2023.

Harten, J. G., Kim, A. M., and Brazier, J. C.: Real and fake data in Shanghai’s informal rental housing market: ground-truthing data scraped from the internet, *Urban Stud.*, <https://doi.org/10.1177/0042098020918196>, 2020.

Hinkel, J., Aerts, J. C. J. H., Brown, S., Jiménez, J. A., Lincke, D., Nicholls, R. J., Scussolini, P., Sanchez-Arcilla, A., Vafeidis, A., and Addo, K. A.: The ability of societies to adapt to twenty-first-century sea-level rise, *Nat. Clim. Change*, 8, 570–578, <https://doi.org/10.1038/s41558-018-0176-z>, 2018.

650 655 IBGE: Monitoramento da variação do nível médio do mar nas estações da Rede Maregráfica Permanente para Geodésia: 2001–2020, Coordenação de Geodésia, Rio de Janeiro, <https://biblioteca.ibge.gov.br/visualizacao/livros/liv101890.pdf>, 2021.

IBGE: História de Macau – Rio Grande do Norte (RN), <https://cidades.ibge.gov.br/brasil/rn/macau/historico>, 2025.

IPCC: Climate change 2022: impacts, adaptation and vulnerability, Contribution of Working Group II to the Sixth Assessment Report of the Intergovernmental Panel on Climate Change, Pörtner, H.-O., Roberts, D. C., Tignor, M., Poloczanska, E. S., Mintenbeck, K., Alegría, A., Craig, M., Langsdorf, S., Löschke, S., Möller, V., Okem, A., and Rama, B. (Eds.), Cambridge Univ. Press, <https://doi.org/10.1017/9781009325844>, 2022.

Jach, T.: Web scraping methods used in predicting real estate prices, in: *Communications in Computer and Information Science*, 375–387, https://doi.org/10.1007/978-3-030-88113-9_30, 2021.

660 Juhász, L., Xu, J., and Parkinson, R. W.: Beyond the tide: a comprehensive guide to sea-level-rise inundation mapping using FOSS4G, *Geomatics*, 3, 522–540, <https://doi.org/10.3390/geomatics3040028>, 2023.



Kaden, U. S.: Floodplain-Inundation-Calculator plugin for QGIS 3, version 0.1, GitHub repository, <https://github.com/usk92/Floodplain-Inundation-Calculator>, <https://doi.org/10.5281/zenodo.6375580>, 2022.

Kelly, B. and Lucio, P. S.: Characterization of risk/exposure to climate extremes for the Brazilian Northeast—case study: Rio Grande do Norte, *Theor. Appl. Climatol.*, 122, 59–67, <https://doi.org/10.1007/s00704-014-1275-z>, 2014.

665 Kendall, M. G.: Rank correlation methods, 4th Edn., Charles Griffin, London, 1975.

Kron, W.: Flood risk = hazard • values • vulnerability, *Water Int.*, 30, 58–68, <https://doi.org/10.1080/02508060508691837>, 2005.

Le Cozannet, G., Garcin, M., Yates, M., Idier, D., and Meyssignac, B.: Approaches to evaluate the recent impacts of sea-level 670 rise on shoreline changes, *Earth-Sci. Rev.*, 138, 47–60, <https://doi.org/10.1016/j.earscirev.2014.08.005>, 2014.

Miller, B. B. and Carter, C.: The test article, *J. Sci. Res.*, 12, 135–147, <https://doi.org/10.1234/56789>, 2015.

López-Dóriga, U. and Jiménez, J. A.: Impact of relative sea-level rise on low-lying coastal areas of Catalonia, NW 675 Mediterranean, Spain, *Water*, 12, 3252, <https://doi.org/10.3390/w12113252>, 2020.

Macedo, Y. M., Felipe, Marinho, A. O., and Victor, P. V. N.: Socio-environmental vulnerability in coastal areas: a case study 680 in the municipality of Macau-RN, Brazil, *Rev. Geociênc. Nordeste*, 11, 708–721, <https://doi.org/10.21680/2447-3359.2025v11n1id38277>, 2025.

Mann, H. B.: Nonparametric tests against trend, *Econometrica*, 13, 245–259, <https://doi.org/10.2307/1907187>, 1945.

MapBiomass: Coleção 9 da série anual de mapas de cobertura e uso da terra do Brasil, <https://brasil.mapbiomas.org/colecoes-mapbiomas/>, last access: 31 July 2025, 2023.

685 Marfai, M. A. and King, L.: Potential vulnerability implications of coastal inundation due to sea level rise for the coastal zone of Semarang city, Indonesia, *Environ. Geol.*, 54, 1235–1245, <https://doi.org/10.1007/s00254-007-0906-4>, 2007.

McGranahan, G., Balk, D., and Anderson, B.: The rising tide: assessing the risks of climate change and human settlements in 690 low elevation coastal zones, *Environ. Urban.*, 19, 17–37, <https://doi.org/10.1177/0956247807076960>, 2007.

Medeiros, F. J., Gomes, R. dos S., Coutinho, M. D. L., and Lima, K. C.: Meteorological droughts and water resources: historical 695 and future perspectives for Rio Grande do Norte state, Northeast Brazil, *Int. J. Climatol.*, <https://doi.org/10.1002/joc.7624>, 2022.

Melo Filho, E.: Meteorological tide at the Brazilian coast, Full Professor thesis, Federal University of Rio Grande, https://sistemas.furg.br/sistemas/sab/arquivos/conteudo_digital/000008808.pdf, 2017.

Morlet, J., Arens, G., Fourgeau, E., and Giard, D.: Wave propagation and sampling theory—Part I: complex signal and 700 scattering in multilayered media, *Geophysics*, 47, 203–221, <https://doi.org/10.1190/1.1441328>, 1982.

Moser, S. C., Ekstrom, J. A., Kim, J., and Heitsch, S.: Adaptation finance archetypes: local governments' persistent challenges 705 of funding adaptation to climate change and ways to overcome them, *Ecol. Soc.*, 24, 28, <https://doi.org/10.5751/ES-10980-240228>, 2019.

Muench, R., Cherrington, E., Griffin, R., and Mamane, B.: Assessment of open access global elevation model errors impact 710 on flood extents in southern Niger, *Front. Environ. Sci.*, 10, <https://doi.org/10.3389/fenvs.2022.880840>, 2022.



NASA Sea Level Projection Tool: IPCC AR6 sea-level-rise projections visualization and data download, <https://sealevel.nasa.gov/ipcc-ar6-sea-level-projection-tool>, last access: 2025, 2021.

Nagy, G. J., Gutiérrez, O., Brugnoli, E., Verocai, J. E., Gómez-Erache, M., Villamizar, A., Olivares, I., Azeiteiro, U. M., Leal Filho, W., and Amaro, N.: Climate vulnerability, impacts and adaptation in Central and South America coastal areas, *Reg. Stud. Mar. Sci.*, 29, 100683, <https://doi.org/10.1016/j.rsma.2019.100683>, 2019.

700 Nicholls, R. J., Wong, P. P., Burkett, V. R., Codignotto, J., Hay, J., McLean, R., Ragoonaden, S., and Woodroffe, C. D.: Coastal systems and low-lying areas, in: *Climate Change 2007: Impacts, Adaptation and Vulnerability, Contribution of Working Group II to the Fourth Assessment Report of the IPCC*, Parry, M. L., Canziani, O. F., Palutikof, J. P., van der Linden, P. J., and Hanson, C. E. (Eds.), Cambridge Univ. Press, Cambridge, 315–356, <https://www.ipcc.ch/site/assets/uploads/2018/02/ar4-wg2-chapter6-1.pdf>, 2007.

705 Nicholls, R. J. and Cazenave, A.: Sea-level rise and its impact on coastal zones, *Science*, 328, 1517–1520, <https://doi.org/10.1126/science.1185782>, 2010.

Olczak, B. and Hanzl, M.: Adaptation to climate change—a challenge for small towns, in: *The urban book series*, 497–520, https://doi.org/10.1007/978-3-031-77752-3_25, 2025.

710 Powell, E. J., Tyrrell, M. C., Milliken, A., Tirpak, J. M., and Staudinger, M. D.: A review of coastal management approaches to support the integration of ecological and human community planning for climate change, *J. Coast. Conserv.*, 23, 1–18, <https://doi.org/10.1007/s11852-018-0632-y>, 2018.

Rabelo, T. O., Túlio, M., Gabriela, I., Luiza, M., Queiroz, L. S., Paulo, , and Pereira, P.: Risk of degradation and coastal flooding hazard on geoheritage in protected areas of the semi-arid coast of Brazil, *Water*, 15, 2564, <https://doi.org/10.3390/w15142564>, 2023.

REDEGEO – App para Rede Geodésica Digital: <http://labsim.unipampa.edu.br/redegeo>, 2020.

Soares, M. and Amaro, V. E.: Geodetic network for coastal monitoring of setentrional littoral of Rio Grande do Norte state, *Bol. Ciênc. Geodésicas*, 17, 571–585, <https://doi.org/10.1590/S1982-21702011000400005>, 2011.

720 Rodríguez, M. G., Nicolodi, J. L., Gutiérrez, O. Q., Cánovas Losada, V., and Espejo Hermosa, A. E.: Brazilian coastal processes: wind, wave climate and sea level, in: *Brazilian Beach Systems*, Short, A. D. and Klein, A. H. da F. (Eds.), Coastal Research Library, vol. 17, Springer, Cham, 37–66, https://doi.org/10.1007/978-3-319-30394-9_2, 2016.

Rouse, H., Bell, R., Lundquist, C., Blackett, P., Hicks, D., and King, D.-N.: Coastal adaptation to climate change in Aotearoa-New Zealand, *N. Z. J. Mar. Freshw. Res.*, 51, 183–222, <https://doi.org/10.1080/00288330.2016.1185736>, 2016.

725 Sanders, B. F., Oliver, , and Bates, P. D.: Flooding is not like filling a bath, *Earth's Future*, 12, e2024EF005164, <https://doi.org/10.1029/2024EF005164>, 2024.

Scardino, G., Anzidei, M., Petio, P., Serpelloni, E., De Santis, V., Rizzo, A., Liso, S. I., Zingaro, M., Capolongo, D., Vecchio, A., Refice, A., and Scicchitano, G.: The impact of future sea-level rise on low-lying subsiding coasts: a case study of Tavoliere delle Puglie (southern Italy), *Remote Sens.*, 14, 4936, <https://doi.org/10.3390/rs14194936>, 2022.



730 Scheiber, L., Hoballah Jalloul, M., Jordan, C. de, Nguyễn, H. Q., and Schlurmann, T.: The potential of open-access data for flood estimations: uncovering inundation hotspots in Ho Chi Minh City, Vietnam, through a normalized flood severity index, *Nat. Hazards Earth Syst. Sci.*, 23, 2313–2332, <https://doi.org/10.5194/nhess-23-2313-2023>, 2023.

735 Shen, Y., Tahvildari, N., Morsy, M. M., Huxley, C., Chen, T. D., and Goodall, J. L.: Dynamic modeling of inland flooding and storm surge on coastal cities under climate change scenarios: transportation infrastructure impacts in Norfolk, Virginia USA as a case study, *Geosciences*, 12, 224, <https://doi.org/10.3390/geosciences12060224>, 2022.

740 Schmid, K.: Mapping and portraying inundation uncertainty of bathtub-type models, *J. Coast. Res.*, 30, 548–561, <https://doi.org/10.2112/JCOASTRES-D-13-00118.1>, 2013.

Smith, K.: Environmental hazards: assessing risk and reducing disaster, 3rd Edn., Routledge, London, 2001.

745 Silva, J.P., Araújo, P.V.N., Diniz, M. T. M., and Santos, J. Y.: Projection and assessment of the physical impacts resulting from sea-level rise by the year 2100 in the urban area of Grossos, *Rev. Geociênc. Nordeste*, 10, 206–214, <https://doi.org/10.21680/2447-3359.2024v10n2id37699>, 2024.

750 Silva, T.C.L., Diniz, M. T. M., Araújo, P.V.N., and Ferreira, B.: Marine hydraulic process modelling using SMC-Brasil on the semi-arid Brazilian coast, *Geosciences*, 15, 344, <https://doi.org/10.3390/geosciences15090344>, 2025.

755 SMC-Brasil – Sistema de Modelagem Costeira: coastal modeling system and data for the Brazilian coast, Environmental Hydraulics Institute (Universidad de Cantabria) / Ministério do Meio Ambiente (Brazil), <http://smcbrasil.ihcantabria.com/downloads/>, last access: 2024, 2025.

760 Soares, Campos, C. C., Bastos, P., Barroso, H. S., Rozane Valente Marins, Teixeira, C., Ozilea, M., de, L., de, M., Caroline Vieira Feitosa, Jorge Iván Sánchez-Botero, Ernesto, L., Cristina, Matthews-Cascon, H., de, F., Adryane Gorayeb, Mariany Sousa Cavalcante, Moro, M., Rossi, S., and Belmonte, G.: Challenges and perspectives for the Brazilian semi-arid coast under global environmental changes, *Perspect. Ecol. Conserv.*, 19, 267–278, <https://doi.org/10.1016/j.pecon.2021.06.001>, 2021.

765 Souza, C. M., Shimbo, J. Z., Rosa, M. R., Parente, L. L., Alencar, A., Rudorff, B. F. T., Hasenack, H., Matsumoto, M., Ferreira, L. G., Souza-Filho, P. W. M., de Oliveira, S. W., Rocha, W. F., Fonseca, A. V., Marques, C. B., Diniz, C. G., Costa, D., Monteiro, D., Rosa, E. R., Vélez-Martin, E., and Weber, E. J.: Reconstructing three decades of land use and land cover changes in Brazilian biomes with Landsat archive and Earth Engine, *Remote Sens.*, 12, 2735, <https://doi.org/10.3390/rs12172735>, 2020.

770 Stephens, S. A., Paulik, R., Reeve, G., Wadhwa, S., Popovich, B., Shand, T., and Haughey, R.: Future changes in built environment risk to coastal flooding, permanent inundation and coastal erosion hazards, *J. Mar. Sci. Eng.*, 9, 1011, <https://doi.org/10.3390/jmse9091011>, 2021.

775 Su, W.-R., Chen, Y.-H., Fu, H.-S., Chang, T.-Y., and Chen, W.-B.: Assessing the inundation risk of cultural heritages along the southwestern coast of Taiwan: present and future, *Reg. Environ. Change*, 24, 2, <https://doi.org/10.1007/s10113-024-02204-9>, 2024.



Terres de Lima, L., Fernández-Fernández, S., Gonçalves, J. F., Magalhães Filho, L., and Bernardes, C.: Development of tools for coastal management in Google Earth Engine: uncertainty bathtub model and Bruun rule, *Remote Sens.*, 13, 1424, <https://doi.org/10.3390/rs13081424>, 2021.

Turner, B. L., Matson, P. A., McCarthy, J. J., Corell, R. W., Christensen, L., Eckley, N., Kasperson, R. E., Luers, A., Lovejoy, T., and Martello, M. L.: A framework for vulnerability analysis in sustainability science, *Proc. Natl. Acad. Sci. USA*, 100, 8074–8079, <https://doi.org/10.1073/pnas.1231335100>, 2003.

Ukoba, K., Onisuru, O. R., Jen, T.-C., Madyira, D. M., and Olatunji, K. O.: Predictive modeling of climate change impacts using artificial intelligence: a review for equitable governance and sustainable outcome, *Environ. Sci. Pollut. Res.*, <https://doi.org/10.1007/s11356-025-36356-w>, 2025.

Vernimmen, R. and Hooijer, A.: New LiDAR-based elevation model shows greatest increase in global coastal exposure to flooding to be caused by early-stage sea-level rise, *Earth's Future*, 11, <https://doi.org/10.1029/2022EF002880>, 2023.

Vital, H.: The mesotidal barriers of Rio Grande do Norte, in: *Geology and Geomorphology of Holocene Coastal Barriers of Brazil*, Muehe, D. (Ed.), Springer, 107, 227–260, https://doi.org/10.1007/978-3-540-44771-9_9, 2009.

Vital, H., Rocha, G. R., and Plácido, J. S.: Morphodynamics of Arrombado tidal inlet, Macau-RN (NE Brazil), *Proc. Coast. Sediments*, 2011, 327–338, https://doi.org/10.1142/9789814355537_0025, 2011.

Vousdoukas, M. I., Mentaschi, L., Voukouvalas, E., Verlaan, M., Jevrejeva, S., Jackson, L. P., and Feyen, L.: Global probabilistic projections of extreme sea levels show intensification of coastal flood hazard, *Nat. Commun.*, 9, 2360, <https://doi.org/10.1038/s41467-018-04692-w>, 2018.

Williams, L. L. and Lück-Vogel, M.: Comparative assessment of the GIS-based bathtub model and an enhanced bathtub model for coastal inundation, *J. Coast. Conserv.*, 24, 2, <https://doi.org/10.1007/s11852-020-00735-x>, 2020.

Wisner, B., Gaillard, J. C., and Kelman, I. (Eds.): *Handbook of hazards and disaster risk reduction*, Routledge, <https://doi.org/10.4324/9780203844236>, 2012.

Yang, L., Jin, T., and Jiang, W.: ASM-SS: the first quasi-global high-spatial-resolution coastal storm surge dataset reconstructed from tide gauge records, *Earth Syst. Sci. Data*, 17, 2793–2807, <https://doi.org/10.5194/essd-17-2793-2025>, 2025.

Yunus, A., Avtar, R., Kraines, S., Yamamoto, M., Lindberg, F., and Grimmond, C.: Uncertainties in tidally adjusted estimates of sea-level rise flooding (bathtub model) for Greater London, *Remote Sens.*, 8, 366, <https://doi.org/10.3390/rs8050366>, 2016.